*Nucleic Acids Research*, 2025, **53**, gkaf134
https://doi.org/10.1093/nar/gkaf134
**RNA and RNA-protein complexes**

# The snoRNP chaperone snR190 and the Npa1 complex form a macromolecular assembly required for 60S ribosomal subunit maturation

**Hussein Hamze[1], Mariam Jaafar[1,2], Ali Khreiss[1,3], Carine Dominique[1], Jessie Bourdeaux[1], Paulo Espirito Santo[1], Alfonso Méndez-Godoy[4], Dieter Kressler[4], Odile Humbert[1], Célia Plisson-Chastang[1], Benjamin Albert[1], Anthony K. Henras[1,*], Yves Henry[1,*]**

[1]Molecular, Cellular and Developmental Biology Unit (MCD), Centre de Biologie Intégrative (CBI), Université de Toulouse, CNRS, 31062 Toulouse, France
[2]Present address: Medpace, 66-70 rue de la Villette, 69003 Lyon, France
[3]Present address: Department of Molecular Biology, University Medical Center Göttingen, Humboldtallee 23, 37073 Göttingen, Germany
[4]Department of Biology, University of Fribourg, Chemin du Musée 10, 1700 Fribourg, Switzerland

*To whom correspondence should be addressed. Email: yves.henry@univ-tlse3.fr
Correspondence may also be addressed to Anthony K. Henras. Email: anthony.henras@univ-tlse3.fr

## Abstract

The early steps of large-ribosomal-subunit assembly feature among the least understood steps of ribosome synthesis in eukaryotes. In *Saccharomyces cerevisiae*, the box C/D chaperone small nucleolar ribonucleoprotein (snoRNP) snR190 and the Npa1 complex, composed of the α-solenoid scaffold proteins Npa1 and Npa2, the DEAD-box helicase Dbp6, the RNA-binding protein Nop8, and Rsa3, are likely involved in early 25S ribosomal RNA (rRNA) folding events. Here, we report for the first time the existence outside pre-ribosomal particles of an independent macromolecular assembly constituted by the Npa1 complex and the chaperone snoRNP snR190. Nop8 mediates the formation of this assembly and can associate on its own with free snR190 snoRNP. Moreover, Nop8 RNA Recognition Motif (RRM) helps tether the snR190 snoRNP to pre-ribosomal particles. The snR190 snoRNA features a specific central stem-loop structure, which is required for high-affinity binding between free snR190 snoRNP and the Npa1 complex. Deleting this extension does not prevent snR190 snoRNA association with pre-ribosomal particles but impairs snR190 activity in early pre-rRNA processing events. This work establishes the importance of association with auxiliary protein complexes for optimum snoRNP chaperone activity during rRNA folding events.

## Graphical abstract

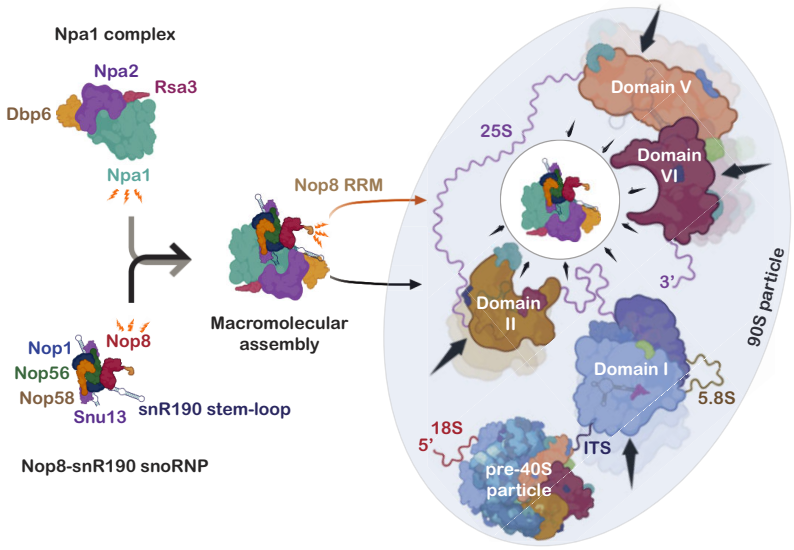


**Received:** August 30, 2024. **Revised:** February 1, 2025. **Editorial Decision:** February 3, 2025. **Accepted:** February 12, 2025

## Introduction

The ribosome is the only cellular machine able to catalyse peptide bond formation during protein synthesis. It is a ribonucleoprotein (RNP) particle composed of a large and a small subunit. Each subunit contains ribosomal RNA (rRNA) associated with ribosomal proteins (RPs). The synthesis of ribosomes involves the production of rRNA precursors (pre-rRNAs), the processing and folding of these precursors, and their assembly with RPs to yield mature functional ribosomal subunits. As the ribosome is a ribozyme, an RNA-based enzyme, one key aspect of its synthesis is the acquisition by the rRNAs of their correct 3D structure, a prerequisite for catalytic activity. In eukaryotes, ribosome biogenesis starts in the nucleolus with the transcription by RNA polymerase I (RNA Pol I) of a polycistronic pre-rRNA. This pre-rRNA is the precursor to the 18S rRNA (present in the small 40S subunit) and the 5.8S and 25S/28S (yeast/higher eukaryotes) rRNAs (present in the large 60S subunit). The large subunit also contains the 5S rRNA which is transcribed independently by RNA Pol III. During transcription, this precursor starts assembling with a subset of RPs as well as scores of so-called assembly factors (AFs) and small nucleolar ribonucleoprotein (snoRNPs) particles. These assembly events on the 5′ part of the nascent RNA Pol I transcript, encompassing the 5′ external transcribed spacer and the 18S rRNA sequence (for a cartoon of pre-rRNA sequence organization, see Supplementary Fig. S1A), lead to the formation of the first pre-ribosomal particle. This particle, termed in the yeast *Saccharomyces cerevisiae* either 90S or 'small subunit processome' (SSU processome) [1, 2], can be visualized as terminal knobs in Miller spreads of rDNA chromatin [3]. The nascent pre-rRNA may be cleaved co-transcriptionally at site A2 within the internal transcribed spacer 1 (ITS1), which separates the 18S and 5.8S rRNA sequences (for a cartoon of pre-rRNA processing steps in *S. cerevisiae*, see Supplementary Fig. S1B). In that scenario, the first independent precursor to the 40S ribosomal subunit, termed the first or primordial pre-40S particle, is released [4]. Meanwhile, assembly events proceed on the 3′ part of the nascent pre-rRNA. Once RNA Pol I transcription is completed, this 3′ part encompasses the remaining ITS1, the 5.8S rRNA sequence, the internal transcribed spacer 2 (ITS2), the 25S rRNA sequence, and the 3′ external transcribed spacer. The association of AFs, RPs, and snoRNPs on this downstream pre-rRNA segment produces the first or primordial pre-60S particle [5]. Cleavage of the pre-rRNA transcript may also occur post-transcriptionally. In that case, a large bi-partite SSU processome/pre-60S particle is generated [5], which will be split into the primordial pre-40S and pre-60S particles by post-transcriptional cleavage within ITS1. The pre-40S and pre-60S particles will then follow independent maturation pathways in the nucleolus, the nucleoplasm, and finally in the cytoplasm to yield the mature 40S and 60S ribosomal subunits competent for translation (for a review of these maturation steps, see [6]).

High-resolution cryo-electron microscopy (cryo-EM) structures of many pre-ribosomal particles have been obtained, revealing the folding of rRNAs at different stages of the maturation pathway and the positioning of AFs, allowing predictions to be made as to their modes of action (for a review, see [7]). The entire primordial pre-60S particle has so far escaped high-resolution structural characterization, likely due to its high intrinsic flexibility [5]. As a consequence, our understanding of the first steps of large-ribosomal-subunit formation lags behind that of other maturation steps. This primordial pre-60S particle contains the 27SA2 pre-rRNA, several box C/D and H/ACA snoRNPs, and ∼40 AFs [5, 8]. Some of these form protein modules, such as the Rrp5/Noc1/Noc2 [9], Npa1/Npa2/Nop8/Dbp6/Rsa3 [10, 11], Erb1/Ytm1/Nop7 [12, 13], and Upa1/Upa2 [5, 14] complexes. In addition, no less than seven proteins belonging to related RNA helicase families (Has1, Mak5, Prp43, Dbp3, Dbp6, Dbp7, and Dbp9) are present within the primordial pre-60S particle. These could promote pre-rRNA folding (see e.g. [15]) and/or regulate snoRNA/pre-rRNA interactions. Indeed, we have recently shown that Dbp7 is involved in the removal of the snR190 box C/D snoRNA [16], a prominent component of the primordial pre-60S particle [5]. All snoRNPs and many of the AFs present in the primordial particle are absent from its maturation product, the nucleolar pre-60S particle containing the 27SB pre-rRNA. High-resolution cryo-EM data could be obtained for this later particle, which showed that only 5.8S rRNA, ITS2, 5′ domains I and II, and part of 3′ domain VI of 25S rRNA were compacted and stabilized at this stage [17–19]. Low-resolution cryo-EM data were also collected for the primordial pre-60S particle [5]. Comparison with the cryo-EM structure of the later 27SB-containing pre-60S particle [18] allowed the identification of ITS2, 5.8S rRNA, and 25S rRNA domains I and II, suggesting that these elements are already stabilized and compacted to a significant extent in the primordial pre-60S particle. This proposal is strengthened by a high-throughput SHAPE probing study [20], which demonstrated that in the primordial pre-60S particle, the ITS2 is already structured, that the root helix of 25S rRNA domain I is formed, and that the base-pairing interactions between 5.8S and 25S rRNAs within domain I are already established. Recently, these conclusions were confirmed by a high-resolution cryo-EM structure of a nascent primordial pre-60S particle encompassing 5.8S rRNA, ITS2, as well as domains I and II of 25S rRNA [21]. Hence, during early steps of large-ribosomal-subunit formation, 25S rRNA domain I is formed and stabilized first, followed by domain II, and then VI. These domains form the solvent-exposed face of the large subunit, onto which the other domains can later assemble.

The molecular functions of most AFs present in the primordial pre-60S particle in these early folding steps remain largely elusive. Most are essential for viability and large-ribosomal-subunit synthesis, underscoring their functional importance. At least 14 of them are necessary for normal steady-state accumulation of the 27SA2 pre-rRNA, indicating that they are necessary for the production and/or stability of the primordial pre-60S particle. These include the Rrp5/Noc1/Noc2 complex [22, 23]; the DExD/H-box proteins Has1 [24], Prp43 [25–27], Dbp3 [28], Dbp7 [29, 30], and Dbp9 [31]; the putative RNA-binding protein Nop4 [32, 33]; and the Npa1/Npa2/Nop8/Rsa3/Dbp6 [10, 11, 34, 35] complex (in the rest of the manuscript referred to as the 'Npa1 complex'). To gain insights into the mechanism of action of these AFs, we and others have searched for their RNA targets using UV Crosslinking and Analysis of cDNA (CRAC) [36]. Binding sites of Npa1 [10], Prp43 [37], and Rrp5 [38] determined by CRAC have been localized next to the binding site of RP Rpl3 in the root helix of 25S rRNA domain I. Npa1 also binds to 25S rRNA domain VI, adjacent to a second Rpl3-binding site, while Dbp6- and Dbp7-binding sites have been identified in 25S rRNA domains III and V, and V and VI, respec-

tively [15, 30]. In addition, CRAC data indicate that Npa1, Prp43, and Rrp5 can be cross-linked to some snoRNAs involved in 25S rRNA modification and it has been proposed that Prp43 controls the interaction of a subset of box C/D snoRNAs with 25S rRNA [37]. Strikingly, Npa1 interacts predominantly with the box C/D snoRNA snR190, which features two rRNA-complementary sequences allowing it to potentially bind to domain I and to the root helix of domain V. Unlike most snoRNAs, snR190 does not guide rRNA modifications and likely functions as an RNA chaperone. We have shown that lack of snR190 snoRNA induces a growth defect and impairs the maturation of the first pre-60S particle [16]. Altogether, these data suggest that the Npa1 complex collaborates with RNA helicases and the chaperone snoRNP snR190 in the folding and/or compaction of 25S rRNA domains I, V, and VI. The hypothesis of a role for Npa1 in the folding of the 3′ end of 25S rRNA is reinforced by the finding that depletion of URB1, the likely human orthologue of Npa1, altered the pre-rRNA conformation around the 3′ end of 28S rRNA [39].

Here, we have investigated the way the Npa1 complex and the snR190 snoRNP interact and the functional implications of this interaction. We provide evidence that the snR190 snoRNP and the Npa1 complex can interact outside pre-ribosomal particles. Nop8 is essential for this interaction. Furthermore, Nop8 or Npa1 depletion weakens snR190 snoRNA association with pre-ribosomal particles, suggesting that they help tether the snR190 snoRNP to these particles. We also show that a specific stem-loop structure in snR190 snoRNA is required for high-affinity binding between free snR190 snoRNA and the Npa1 complex. While this stem-loop structure is not required for snR190 snoRNA association with pre-60S particles, our results suggest that it is important for snR190 snoRNP chaperone function during early pre-rRNA processing steps.

## Materials and methods

### Plasmids

Centromeric plasmids based on pHA113 [40] expressing Nop8 or Nop8ΔRRM were obtained as follows. A plasmid expressing Nop8 tagged with two IgG-binding domains of *Staphylococcus aureus* protein A was obtained by amplifying *NOP8* open reading frame using *S. cerevisiae* genomic DNA with appropriate primers (Supplementary Table S1) followed by cloning in the BamHI site of pHA113 using the In-Fusion system (Clontech). The resulting plasmid, pHA113-*NOP8*-ZZ, was used as template to generate plasmids pHA113-*NOP8* and pHA113-*NOP8ΔRRM*-ZZ using the In-Fusion system (Clontech) and appropriate primers (Supplementary Table S1). Finally, pHA113-*NOP8ΔRRM*-ZZ was used as template to generate plasmid pHA113-*NOP8ΔRRM* using the In-Fusion system (Clontech) and appropriate primers (Supplementary Table S1). The *NOP8* or *NOP8ΔRRM* open reading frames inserted in the resulting plasmids were entirely sequenced.

Plasmids YCplac22-*NOP8*-HTP (pDK10780; for expression of Nop8-HTP under the control of the *NOP8* promoter) and YCplac22-*NOP8.81C*-HTP (pDK10781; for expression of Nop8ΔRRM-HTP under the control of the *NOP8* promoter; 81C denotes that the encoded Nop8ΔRRM starts with amino acid 81 of Nop8 and ends at the native C-terminus) were constructed by subcloning a 2.43 kb EcoRI/HindIII fragment from YCplac111-*NOP8*-HTP (pDK10712) or a 2.19 kb EcoRI/HindIII fragment from YCplac111-*NOP8.81C*-HTP (pDK10713) into YCplac22-*RPL10* (pDK5026; [41]). YCplac111-*NOP8*-HTP (pDK10712) was constructed by cloning a 1.78 kb EcoRI/BamHI-digested P*NOP8-NOP8* polymerase chain reaction (PCR) product, amplified from template YCplac111-*NOP8* (pDK510; [42]) with oligonucleotides ODK3867 and ODK3285 (Supplementary Table S1), into YCplac111-*NSA1*-HTP (pDK2261; [43]). YCplac111-*NOP8.81C*-HTP (pDK10713) was constructed by cloning a 1.54 kb EcoRI/BamHI-digested P*NOP8-NOP8.81C* fusion PCR product, amplified from template YCplac111-*NOP8*-T*ADH1* (pDK10487) with oligonucleotides ODK838 and ODK3880 (5′ PCR) and ODK3879 and ODK389 (3′ PCR) (Supplementary Table S1), into YCplac111-*NSA1*-HTP (pDK2261). YCplac111-*NOP8*-T*ADH1* (pDK10487) was constructed by cloning a 1.78 kb EcoRI/BamHI-digested P*NOP8-NOP8* PCR product, amplified from template YCplac111-*NOP8* (pDK510) with oligonucleotides ODK3867 and ODK3285 (Supplementary Table S1), into pADH111-*LTV1* (pDK3331).

To obtain plasmids expressing Nop8-NeonGreen (Nop8-NG) or Nop8ΔRRM-NeonGreen (Nop8ΔRRM-NG), we proceeded as follows. A NeonGreen cassette amplified by PCR with BamHI_FOR_NG and XhoI_REV_NG oligonucleotides (Supplementary Table S1) was digested with BamHI and XhoI and ligated with the BamHI/XhoI-digested 8-kb fragments from plasmids YCplac22-*NOP8*-HTP and YCplac22-*NOP8.81C*-HTP, resulting in plasmids p*NOP8*-NG and p*NOP8ΔRRM*-NG, respectively.

Construction of plasmids expressing snR190 wild-type (WT) and snR190-[mut.AB] mutant was described in [16]. Plasmids expressing snR190 mutants snR190-[mut.B], snR190-[short Δstem], snR190-[intermediate Δstem], and snR190-[large Δstem], were obtained by mutagenesis of the plasmid expressing WT snR190 (pCH32 vector + WT *U14-SNR190* gene insert, [16]) using the PCR-based In-Fusion mutagenesis system (Clontech) and appropriate primers for each mutant (Supplementary Table S1). The original template plasmid was then eliminated by the 'Cloning Enhancer' treatment (Clontech) and the linear PCR products were circularized using the In-Fusion system before transformation into competent *Escherichia coli* cells (Stellar, Clontech). To generate a plasmid expressing snR190-[mut.B-large Δstem], a mutation in box B was introduced using the above protocol in the plasmid expressing snR190-[large Δstem]. All resulting plasmids were verified by sequencing.

### Yeast strains

A BY4742 (*MATα*, *his3Δ1*, *leu2Δ0*, *lys2Δ0*, and *ura3Δ0*) strain expressing Noc1-FPZ (Flag-PreScission cleavage site-tandem IgG-binding Z domains derived from *S. aureus* protein A) was produced by transforming BY4742 with a PCR cassette obtained with plasmid pBS1479-NAT-2XFlag-PPX-ZZ and primers listed in Supplementary Table S2. Clones having integrated the nourseothricin resistance gene were selected on Yeast extract Peptone (YP) medium supplemented with 2% glucose and nourseothricin (Jena Bioscience, 80 μg/ml final concentration). *GAL::HA-npa1/NOC1::FPZ*

and *GAL::HA-nop8/NOC1::FPZ* strains (BY4742 background) were produced by transforming the above described Noc1-FPZ-expressing strain with PCR cassettes obtained with plasmid pFA6a-kanMX6-PGAL1-3HA [44] and primers listed in Supplementary Table S2. Clones having integrated the kanMX6 resistance gene were selected on YP medium supplemented with 2% galactose and G418 (Gibco, 200 μg/ml final concentration). An *snr190-[mut.C]* strain [16] expressing Nop8-FPZ was produced as described above using primers listed in Supplementary Table S2. Strains expressing Nop8-HTP (HTP consists of a (His)6 tag, a TEV protease cleavage site, and two Z domains from *S. aureus* protein A) or Nop8ΔRRM-HTP under the control of the *NOP8* promoter were obtained upon transformation of the *NOP8* shuffle strain YAM1357 (*MAT***a**, *nop8*::HIS3MX4, *ade3*::kanMX4, pHT4467Δ-*NOP8*; W303 background) with plasmid YCplac22-*NOP8*-HTP (pDK10780) or YCplac22-*NOP8.81C*-HTP (pDK10781) and subsequent counter-selection on plates containing 5-FOA. Strains expressing Nop1-mCherry and Nop8-NG or Nop8ΔRRM-NG were obtained by transforming strain *GAL::HA-nop8* with plasmids pUN100NOP1::mCherry [45] and p*NOP8*-NG or p*NOP8ΔRRM*-NG, respectively. A *GAL::HA-nop8* strain was produced by transforming strain MW3628 (*MAT*α, *ura3-52*, *his3-Δ200*, *trp1-Δ63*, and *leu2-Δ1*) [46] with a PCR cassette obtained with plasmid pFA6a-kanMX6-PGAL1-3HA [44] and primers listed in Supplementary Table S2. Clones having integrated the kanMX6 resistance gene were selected on YP medium supplemented with 2% galactose and G418 (Gibco, 200 μg/ml final concentration).

Construction of the *RSA3::FPZ*, *DBP6::FPZ*, *NPA2::FPZ*, *NOP8::FPZ*, *GAL::HA-npa1/RSA3::FPZ*, *GAL::HA-npa1/DBP6::FPZ*, *GAL::HA-npa1/NPA2::FPZ*, *GAL::HA-npa1/NOP8::FPZ*, *GAL::HA-nop8/RSA3::FPZ*, and *rrn3.8/RSA3::FPZ* strains was described in [10]. Strains *rrn3.8/GAL::HA-npa1/RSA3::FPZ* and *rrn3.8/GAL::HA-npa2/RSA3::FPZ* were produced by transforming the *rrn3.8/RSA3::FPZ* strain with PCR cassettes obtained with plasmid pFA6a-kanMX6-PGAL1-3HA [44] and primers listed in Supplementary Table S2. Strain *rrn3.8/RSA3::FPZ/snr190-[mut.C]* was obtained by crossing haploid strains *rrn3.8/RSA3::FPZ* and *snr190-[mut.C]* [16], sporulation of the resulting diploids and tetrad dissections. The correct haploid strains were selected on the basis of temperature sensitivity and resistance to nourseothricin; moreover, mutation of the *SNR190* gene was verified by sequencing a locus-specific PCR product and confirmed by northern analysis. An *snr190-[mut.C]* strain expressing Nop7-TAP (TAP consists of a calmodulin-binding peptide tag, a TEV protease cleavage site, and two Z domains from *S. aureus* protein A) was constructed by transforming a *snr190-[mut.C]* strain [16] with a PCR fragment obtained using genomic DNA from a *NOP7::TAP* strain (Yeast TAP-Tagged ORF collection, Horizon Discovery) and primers listed in Supplementary Table S2.

All strains used in this work are listed in Supplementary Table S4.

## Immunoprecipitation experiments

Immunoprecipitation experiments with IgG Sepharose were performed as described in [16].

## RNA extractions and northern blot analyses

Yeast total RNAs were extracted as described in [16]. Northern blot analyses of high- and low-molecular weight RNAs were performed as described in [16]. Sequences of antisense oligonucleotides used to detect snR190, snR5, snR37, and snR42 snoRNAs are listed in [8, 16] and those used to detect snR3 and snR39b snoRNAs in Supplementary Table S3. The sequences of oligonucleotides 23S1 used to detect 35S, 32S, and 27SA2 pre-rRNAs and rRNA2.1 used to detect 35S, 32S, 27SA2, and 27SB pre-rRNAs have been reported in [16].

## Tandem affinity purifications

Yeast cell powder was produced using a PM 100 planetary ball mill (Retsch) from a cell pellet obtained from 6 l of yeast culture grown to an $OD_{600}$ of 0.6–0.8. A total of 6 g of cell powder was dissolved in 8 ml of buffer A [20 mM Tris–HCl (pH 8), 200 mM KCl, 5 mM MgAc, 0.2% Triton X-100, 1 mM DTT] to which cOmplete EDTA-free protease inhibitor cocktail (Roche) and RiboLock RNase inhibitor (Thermo Scientific) were added. The sample was centrifuged in a Beckman Coulter Optima XE-100 ultracentrifuge at 4°C for 2 h at 39 000 rpm in a Beckman Ti50.2 rotor. The resulting supernatant was subjected to a second ultracentrifugation step during 45 min at 39 000 rpm at 4°C. When tandem affinity purifications were perfomed with *rrn3.8* cells, the two ultracentrifugation steps were omitted and replaced by a centrifugation step in a Beckman Coulter Avanti J-26 XP centrifuge at 4°C for 15 min in a Beckman JA-20 rotor. Then, 9 ml of clarified extract were loaded on a 20-ml column (Bio-Rad) containing 200 μl (bead volume) IgG Sepharose beads (6 Fast Flow, Cytiva). The beads were incubated with the extract during 1 h 30 min at 4°C with gentle agitation. Beads were then washed with 60 ml of buffer B [50 mM Tris–HCl (pH 7.4), 200 mM KCl, 5 mM MgAc, 0.2% Triton X-100, 1 mM DTT], then incubated overnight in a 15-ml Falcon tube at 4°C with 50 units of PreScission protease (Cytiva) in 3 ml of buffer B supplemented with 80 units of RiboLock RNase inhibitor (Thermo Scientific). The sample was centrifuged 2 min at 1200 rpm in an Eppendorf 5810 R benchtop centrifuge and the supernatant was collected. The IgG Sepharose beads were mixed with 2 ml of buffer B and centrifuged 2 min at 1200 rpm in an Eppendorf 5810 R benchtop centrifuge. The supernatant was collected and mixed with the previously collected supernatant. The resulting sample was applied to a 10-ml Bio-Rad column containing 100 μl (bead volume) of anti-Flag M2 affinity gel (Sigma) and incubated with the gel for 1 h at 4°C on a rotating wheel. The column was washed with 40 ml of buffer C [10 mM Tris–HCl (pH 7.4), 150 mM NaCl, 5 mM $MgCl_2$, 1 mM DTT]. Purified complexes were eluted by adding five times 200 μl of buffer C supplemented with 2x Flag peptide (400 μg/ml, IGBMC Strasbourg). Alternatively, the gel was mixed with 1 ml of buffer C and two 550-μl aliquots were transferred to two 1.5-ml Eppendorf tubes. The tubes were centrifuged 1 min, 2000 rpm in an Eppendorf 5415 R benchtop centrifuge and the supernatant was discarded. RNAs were extracted from the bead pellet of one sample. The beads of the other sample were directly mixed with 50 μl of sodium dodecyl sulfate (SDS) sample buffer [100 mM Tris–HCl (pH 8.0), 4% SDS, 20% glycerol, 0.04% bromophenol blue, 200 mM DTT] for protein analysis.

### pCp labelling

RNAs were labelled with 10 μCi [$^{32}$P]pCp (PerkinElmer) and 10 units of T4 RNA ligase (Thermo Scientific) in the presence of 40 units of RNasin ribonuclease inhibitor (Promega) in a 20 μl reaction volume at 4°C overnight. Labelled RNAs were phenol/chloroform extracted, ethanol precipitated, washed, and resuspended in 50% formamide (v/v). The labelled RNAs were electrophoresed in Tris–Borate–ethylenediaminetetraacetic acid buffer on a 6% acrylamide/bis-acrylamide (19:1)/50% urea (w/v) gel for 3 h at 1800 V. The gel was dried on 3MM paper and exposed to a phosphorimager screen.

### Western blot analyses

Western blot analyses were performed as described in [15, 16]. FPZ-tagged or TAP-tagged proteins were detected with rabbit peroxidase anti-peroxidase (PAP) soluble complex (Sigma) (1:10 000 dilution). Primary antibodies used to detect Npa1 (1:2000 dilution), Dbp6 (1:10 000 dilution), Nop8 (1:1000 dilution), and Nhp2 (1:5000 dilution) were generated in rabbits by custom antibody production services and described elsewhere [10, 40]. Yeast Nop1 was detected with anti-*Xenopus laevis* Fibrillarin antibodies (1:270 dilution) raised in rabbits. Anti-rabbit IgG-HRP conjugate (Promega) were used when needed as secondary antibodies (1:10 000 dilution).

### Fluorescence microscopy

Fluorescence microscopy and image quantifications were performed as described in [47].

## Results

### Npa1 or Nop8 depletion perturbs the association of snR190 snoRNA with pre-ribosomal particles

We previously showed that snR190 snoRNA inactivation affects the association of Npa1 complex members with pre-ribosomal particles [16]. We wanted to determine whether the reverse was also true, i.e. whether Npa1 complex inactivation impacts snR190 snoRNA association with pre-ribosomal particles. To test this hypothesis, we immunoprecipitated 90S and early pre-60S pre-ribosomal particles using tagged Noc1 (Noc1-FPZ) as bait and extracts from WT cells and cells depleted of Npa1, which is essential for Npa1 complex formation [10]. Npa1 depletion was achieved through the use of cells conditionally expressing the *NPA1* gene from a *GAL1-10* promoter that can be turned off by shifting cells to a glucose-containing medium. The co-precipitation efficiency of snR190 snoRNA was then analysed by northern blot (Fig. 1A). As controls, we also assessed the co-precipitation efficiency of a subset of snoRNAs, which are either efficiently cross-linked to Npa1 (snR5 and snR42), moderately so (snR39b), or hardly at all (snR3) in CRAC experiments [10]. Npa1 depletion decreased the co-precipitation efficiency of all snoRNAs tested (Fig. 1A). This was neither due to reduced precipitation of tagged Noc1 (Fig. 1A), nor to lack of co-precipitation of pre-rRNAs (Supplementary Fig. S2A) in absence of Npa1. Strikingly, the co-precipitation efficiency of snR190 snoRNA was reduced the most in absence of Npa1 (10-fold reduction), while that of the other snoRNAs was significantly less affected (two- to three-fold reduction) (Fig. 1A).

We then assessed whether lack of Nop8 also has a specific impact on snR190 snoRNA association with pre-ribosomal particles. Strikingly, while Nop8 depletion did not affect precipitation of Noc1-FPZ (Fig. 1B) nor the co-precipitation of pre-rRNAs (Supplementary Fig. S2B), it reduced snR190 snoRNA co-precipitation to background levels (Fig. 1B). The co-precipitation of other snoRNAs tested was also affected, but to a far lesser extent.

We also analysed the effect of depleting Dbp6, the DEAD-box ATPase component of the Npa1 complex [15], on snR190 snoRNA association with pre-ribosomal particles. Contrary to the lack of Nop8, Dbp6 depletion had little effect on snR190 snoRNA co-precipitation with Noc1-FPZ (Supplementary Fig. S3).

We further assessed the effect of Npa1 or Nop8 depletion on snR190 snoRNA association with pre-ribosomal particles by sedimentation experiments on sucrose gradients (Supplementary Fig. S4). Neither Npa1 nor Nop8 depletion completely prevented a fraction of snR190 snoRNA from co-sedimenting with pre-rRNA components of 60S subunit precursors (35S, 32S, and 27SB pre-rRNAs). However, Npa1 and Nop8 depletions led to a specific two- and four-fold increase, respectively, in the sedimentation of snR190 snoRNA in light fractions (i.e. not pre-ribosome bound), consistent with weakened association with pre-ribosomal particles. In agreement with immunoprecipitation results, the effect is stronger in the case of Nop8 depletion than Npa1 depletion.

We conclude that Npa1 and Nop8 are specifically required for the stable association of snR190 snoRNA with pre-ribosomal particles, while Dbp6 is not. Besides Npa1, for which a direct interaction with snR190 snoRNA could be revealed by CRAC [10], Nop8 therefore also seems to play a key role in snR190 snoRNA integration and/or retention within early pre-60S pre-ribosomal particles.

### The snR190 snoRNP interacts with the Npa1 complex outside pre-ribosomal particles

The mutual dependence of the Npa1 complex and snR190 snoRNA for their stable association with pre-ribosomal particles ([16] and this work) may be due to the fact that they are integrated as a pre-formed module into the particles. We therefore tested whether snR190 snoRNA is associated with the Npa1 complex outside pre-ribosomal particles. To purify the free Npa1 complex, we used a strain in which RNA Pol I can be inactivated conditionally, abrogating *de novo* pre-ribosomal particle production. This strain (*rrn3.8*) expresses a temperature-sensitive version of the Rrn3 RNA Pol I transcription factor. At 25°C, RNA Pol I is active and pre-ribosomal particles are produced and matured. After transfer for 4 h to 37°C, RNA Pol I transcription is shut down and pre-ribosomal particles are hardly detectable (Supplementary Fig. S5A). We proceeded to tandem affinity purification of the Npa1 complex using an FPZ-tagged version of Rsa3 from *rrn3.8* cells, or WT cells as controls, all grown at 37°C. Northern analysis confirmed the absence of pre-rRNAs in the sample purified from *rrn3.8* cells grown at 37°C (Supplementary Fig. S5B), while western analysis indicated that in the same conditions, all Npa1 complex members were co-purified with Rsa3-Flag, even if Dbp6 was underrepresented (Supplementary Fig. S5C). Strikingly, only the snR190 snoRNA was efficiently co-purified with Rsa3-Flag from *rrn3.8* cells grown at 37°C, as shown by northern blot (Fig. 2A) and pCp labelling (Fig. 2B). These data indicate that snR190 snoRNA can specifically interact with the Npa1

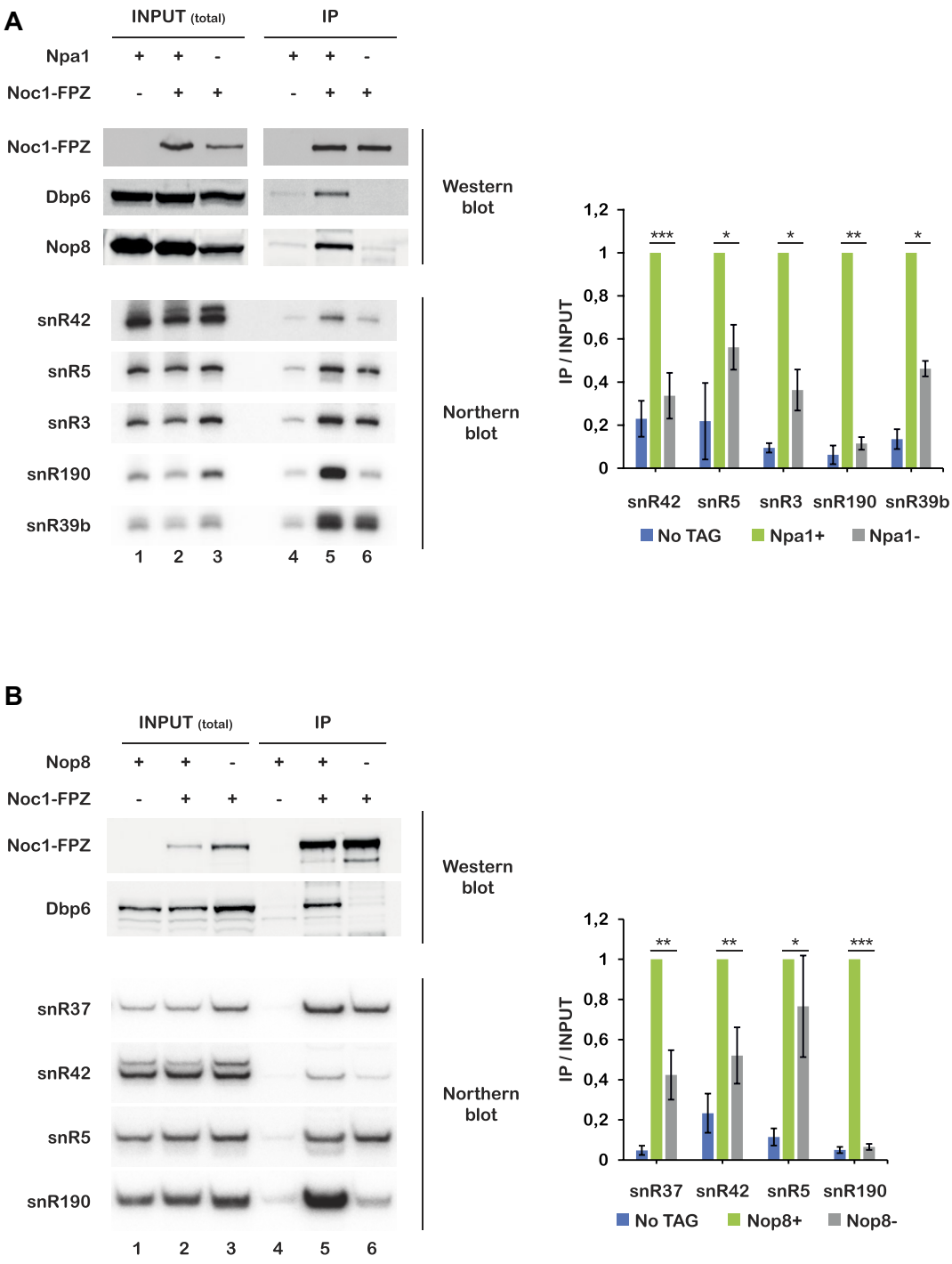


**Figure 1.** Npa1 or Nop8 depletion strongly affects the association of snR190 snoRNA with pre-ribosomal particles. Immunoprecipitation experiments were carried out using IgG Sepharose and extracts from a BY4742 WT strain [labelled Npa1+, Noc1-FPZ− (**A**) or Nop8+, Noc1-FPZ− (**B**)], a strain expressing Noc1-FPZ (i.e. Noc1 bearing a C-terminal Flag tag, followed by a PreScission cleavage site and two IgG-binding Z domains of *S. aureus* protein A) [labelled Npa1+, Noc1-FPZ+ (panel A) or Nop8+, Noc1-FPZ+ (panel B)], a *GAL::HA-npa1/NOC1::FPZ* strain [labelled Npa1−, Noc1-FPZ+ (panel A)], or a *GAL::HA-nop8/NOC1::FPZ* strain [labelled Nop8−, Noc1-FPZ+ (panel B)] expressing Noc1-FPZ and depleted of either Npa1 or Nop8, respectively, following growth in glucose-containing medium for 14 h. Total proteins or RNAs were extracted from input extracts [INPUT (total)] or from immunoprecipitated samples (IP) and analysed by western blot (top panels) or northern blot (bottom panels), respectively. Noc1-FPZ was detected using PAP, Dbp6 and Nop8 with specific antibodies. The indicated snoRNAs were detected by northern blot using antisense oligonucleotide probes. Quantifications of northern data are presented in the histograms on the right. Ratios of precipitated snoRNAs versus total snoRNAs present in the input extracts (IP/INPUT) were computed from phosphorimager scans of northern membranes. Ratios obtained for the non-depleted strains expressing Noc1-FPZ were arbitrarily set at 1. Error bars correspond to standard deviations computed from three independent biological replicates. Statistically significant differences determined using one-tailed paired Student's *t*-test are indicated by asterisks (***$P < .001$; **$P < .01$; *$P < .1$).

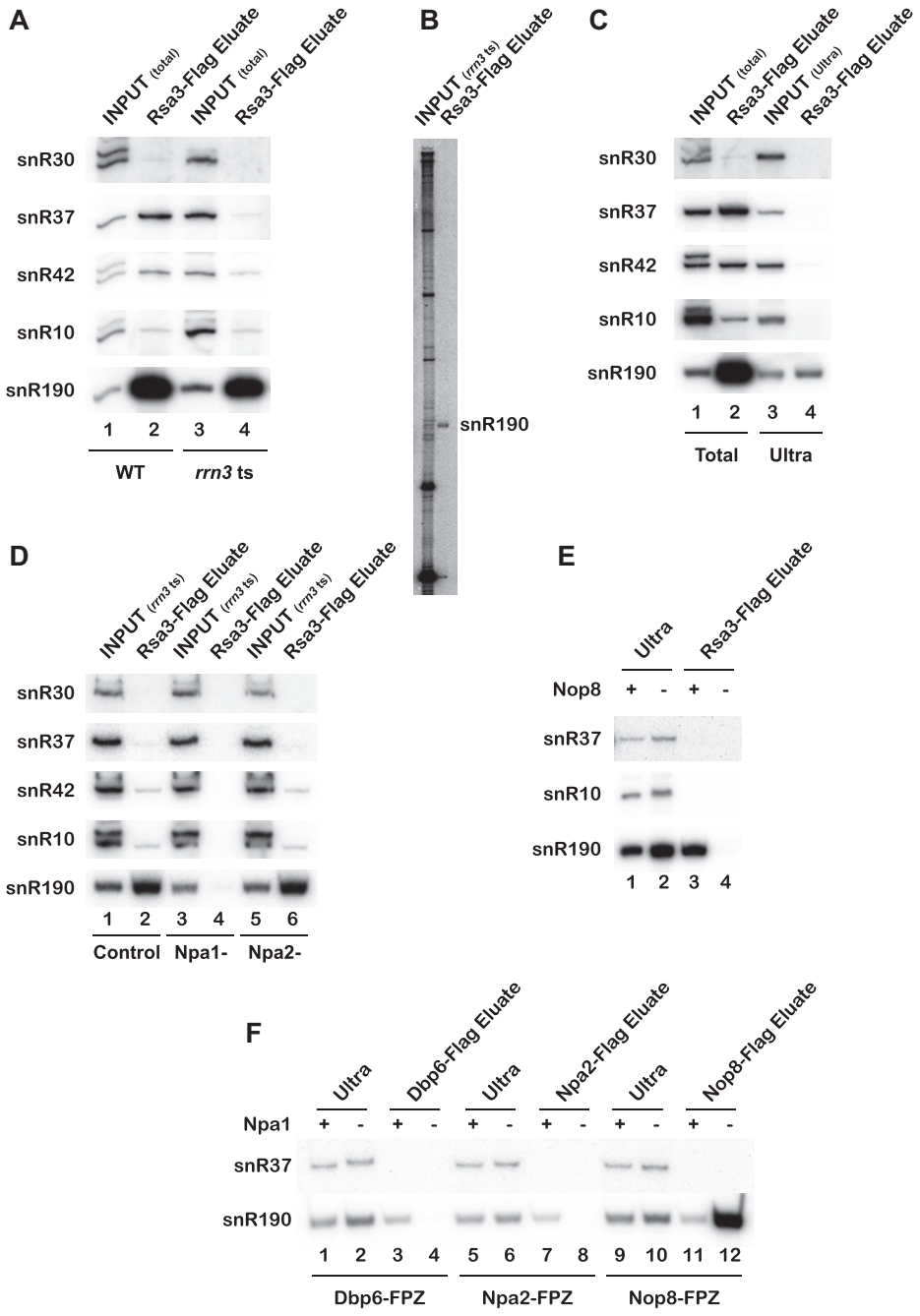


**Figure 2.** (A–C) snR190 snoRNA specifically interacts with the isolated Npa1 complex. (**A, B**) Rsa3-FPZ was subjected to tandem affinity purification from extracts of *RSA3::FPZ* (WT) or *rrn3.8/RSA3::FPZ* (*rrn3* ts) cells grown at 37°C for 4 h. RNAs from the initial total clarified extracts [INPUT (total)] or from the eluates from the anti-Flag affinity columns (Rsa3-Flag eluate) were analysed by northern blot, using oligonucleotide probes complementary to the indicated snoRNAs (panel A) or, solely in the case of samples obtained from *rrn3.8/RSA3::FPZ* (*rrn3* ts) cells, by pCp labelling (panel B). (**C**) Tandem affinity purification of Rsa3-FPZ was carried out with a WT *Rsa3::FPZ* strain extract not subjected (total) or subjected to two consecutive rounds of ultracentrifugation (ultra). RNAs extracted from the initial clarified extracts (INPUT) and from the eluates from the anti-Flag affinity columns (Rsa3-Flag eluate) were analysed by northern blot, using oligonucleotide probes complementary to the indicated snoRNAs. (**D**) Nap1, but not Npa2, is required for the interaction between tagged Rsa3 and snR190 snoRNA. Rsa3-FPZ was subjected to tandem affinity purification from extracts of *rrn3.8/RSA3::FPZ* (control, lanes 1 and 2), *rrn3.8/GAL::HA-npa1/RSA3::FPZ* (Npa1−, lanes 3 and 4), or *rrn3.8/GAL::HA-npa2/RSA3::FPZ* (Npa2−, lanes 5 and 6) strains grown in glucose-containing medium at 37°C for 8 h. RNAs from the initial total clarified extracts [INPUT (*rrn3* ts)] or from the eluates from the anti-Flag affinity columns (Rsa3-Flag eluate) were analysed by northern blot with probes complementary to the indicated snoRNAs. (**E**) Nop8 is required for the interaction between tagged Rsa3 and snR190 snoRNA. Tandem affinity purification of Rsa3-FPZ was carried out with soluble extracts, obtained after two ultracentrifugation steps, from *RSA3::FPZ* (Nop8+) or *GAL::HA-nop8/RSA3::FPZ* (Nop8−) cells grown in glucose-containing medium for 14 h. RNAs from these extracts (ultra) or from the anti-Flag affinity column eluate (Rsa3-Flag eluate) were analysed by northern blot with probes complementary to the indicated snoRNAs. (**F**) Nop8 interacts with snR190 snoRNA in absence of Npa1 complex formation. Tandem affinity purification of FPZ-tagged proteins was carried out with soluble extracts, obtained after two ultracentrifugation steps, from *DBP6::FPZ*, *NPA2::FPZ*, and *NOP8::FPZ* cells (all labelled 'Npa1+') or *GAL::HA-npa1/DBP6::FPZ*, *GAL::HA-npa1/NPA2::FPZ*, and *GAL::HA-npa1/NOP8::FPZ* cells (all labelled 'Npa1−') grown in glucose-containing medium for 14 h. RNAs from these extracts (ultra) or from the anti-Flag affinity column eluates (Flag eluate) were analysed by northern blot with probes complementary to the indicated snoRNAs.

complex when it is not associated with pre-ribosomal particles. To rule out the possibility that such interaction only occurs in cells in which RNA Pol I transcription has been abolished, we repeated the tandem affinity purification of the Rsa3-FPZ bait protein from an extract of a WT strain that was subjected to two consecutive ultracentrifugation steps to pellet pre-ribosomal particles, as previously described [10] (see also Supplementary Fig. S6A). Northern analysis showed that only snR190 snoRNA was specifically co-purified with tagged Rsa3 (Fig. 2C) and the other Npa1 complex members (Supplementary Fig. S6B) under these conditions.

Given the specific association between the snR190 snoRNA and the isolated Npa1 complex, we assessed whether snR190 snoRNA contributes to the cohesion of the free Npa1 complex. We performed a tandem affinity purification of tagged Rsa3 from *rrn3.8* cells expressing or lacking snR190 snoRNA and grown at 37°C. The co-purification of Npa1 and Dbp6 with tagged Rsa3 is not diminished by the absence of snR190 snoRNA (Supplementary Fig. S7A). Strikingly, as previously observed [16], lack of snR190 snoRNA induces a clear drop in the steady-state level of Nop8 (Supplementary Fig. S7A, compare lanes 1 and 2). Nevertheless, Nop8 is co-purified with tagged Rsa3 in absence of snR190 snoRNA. These data suggest that snR190 snoRNA is not required for the association between Rsa3 and at least Npa1 and Dbp6 outside pre-ribosomal particles.

The co-purification with Rsa3 of the methyltransferase Nop1, a known component of the snR190 snoRNP [48], only in the presence of snR190 snoRNA, but not of Nhp2, a core component of box H/ACA snoRNPs [49], strengthens the conclusion that the snR190 snoRNP associates with the free Npa1 complex (Supplementary Fig. S7B).

## The snR190 snoRNP is tethered to the free Npa1 complex via Npa1 and Nop8

CRAC data indicated that Npa1 directly binds to snR190 snoRNA [10], strongly suggesting that the snR190 snoRNP is tethered to the Npa1 complex via at least Npa1. We next assessed the contribution of the other members of the Npa1 complex to the interaction with snR190 snoRNA. We first analysed the consequence of Npa2 or Npa1 depletion on the ability of snR190 snoRNA to interact with Rsa3-FPZ when *de novo* ribosome biogenesis is inhibited. For this analysis, we used *rrn3.8/GAL::HA-npa1/RSA3::FPZ* or *rrn3.8/GAL::HA-npa2/RSA3::FPZ* strains grown in glucose-containing medium at 37°C to inactivate RNA Pol I transcription and deplete Npa1 or Npa2, respectively. When Npa1 was depleted, Npa1 complex formation was inhibited (Supplementary Fig. S8A), as also shown previously [10] and snR190 snoRNA failed to be co-purified with Rsa3 (Fig. 2D, lanes 3 and 4). In absence of Npa2, an Npa1/Nop8/Rsa3 sub-complex could form (Supplementary Fig. S8A), consistent with our previous findings [10] and snR190 snoRNA was efficiently co-purified with this module (Fig. 2D, lanes 5 and 6). Thus, Npa2 is dispensable for snR190 snoRNA interaction with the Npa1 complex.

Given the importance of Nop8 for snR190 snoRNA association with pre-ribosomal particles (Fig. 1B), we next assessed the effect of Nop8 depletion on the ability of snR190 snoRNA to interact with the isolated Npa1 complex. Tandem affinity purification of Rsa3-FPZ from Nop8-depleted cells after two ultracentrifugation steps to pellet pre-ribosomal particles showed that snR190 snoRNA does not co-purify with the Npa1/Npa2/Dbp6/Rsa3 sub-complex (Supplementary Fig. S8B and Fig. 2E). These results indicate that Nop8 is essential for the interaction of snR190 snoRNA with the free Npa1 complex.

The above data point out that Rsa3 on its own cannot interact with snR190 snoRNA. To determine whether the other Npa1 complex members, Dbp6, Npa2, or Nop8 can interact on their own with the free snR190 snoRNP, we depleted Npa1 to prevent Npa1 complex formation and assessed whether snR190 snoRNA could be co-purified with FPZ-tagged Dbp6, Npa2, or Nop8 from soluble extracts obtained after two ultracentrifugation steps to pellet pre-ribosomes (Supplementary Fig. S8C). Northern data indicated that when Npa1 is expressed, snR190 snoRNA was specifically co-purified with tagged Dbp6, Npa2, and Nop8 (Fig. 2F, lanes 3, 7, and 11), further strengthening the conclusion that snR190 snoRNA is specifically associated with the isolated Npa1 complex. In contrast, Npa1 depletion severely reduced the efficiency of snR190 snoRNA co-purification with tagged Dbp6 or Npa2 (Fig. 2F, lanes 4 and 8). Strikingly however, the interaction between tagged Nop8 and snR190 snoRNA was enhanced in absence of Npa1 (Fig. 2F, compare lanes 11 and 12), strongly suggesting that Nop8 directly binds to the snR190 snoRNP.

We conclude from these analyses that the snR190 snoRNP is tethered to the free Npa1 complex via Npa1 and Nop8.

## Nop8 RNA recognition motif strengthens snR190 snoRNA association with pre-ribosomal particles

Nop8 contains an RNA recognition motif (RRM) at its N-terminus [50, 51]. We reasoned that Nop8 might connect the Npa1 complex to snR190 snoRNA via this RRM. To test this hypothesis, we performed immunoprecipitation experiments with whole-cell extracts of strains expressing tagged versions of Nop8 lacking the RRM (Nop8ΔRRM), or WT Nop8 as control and assessed the extent of snR190 snoRNA co-precipitation. Nop8ΔRRM accumulated and was precipitated to the same extent as full-length Nop8 (Fig. 3A) and snR190 snoRNA was co-precipitated with Nop8ΔRRM nearly as well as with full-length Nop8 (Fig. 3B). In contrast, the co-precipitation efficiency of snR37 with Nop8ΔRRM dropped three-fold compared with the WT situation, which might reflect a decreased co-precipitation of pre-ribosomal particles. Indeed, high molecular weight northern data showed that deletion of the RRM reduced the co-precipitation efficiency of the 35S, 32S, and 27SA2 pre-rRNAs ~2-fold (Fig. 3C). These data demonstrate that the RRM motif is dispensable for Nop8 interaction with snR190 snoRNA but likely strengthens its association with the pre-rRNAs.

Given that Nop8 is crucial for snR190 snoRNA association with pre-ribosomal particles, we next tested whether the deletion of its RRM reduces snR190 snoRNA pre-ribosome association. We immunoprecipitated pre-ribosomal particles via Noc1-FPZ from extracts of *GAL::HA-nop8/NOC1::FPZ* cells depleted of genome-encoded Nop8 and expressing Nop8ΔRRM, or, as control, WT Nop8 from plasmids. Nop8ΔRRM displayed reduced co-precipitation with Noc1-FPZ (Fig. 4A), suggesting weakened association with pre-ribosomal particles. Co-precipitation of snR190 snoRNA with Noc1-FPZ dropped three-fold under conditions of Nop8ΔRRM expression, providing evidence of weakened snR190 snoRNA association with pre-ribosomal parti-

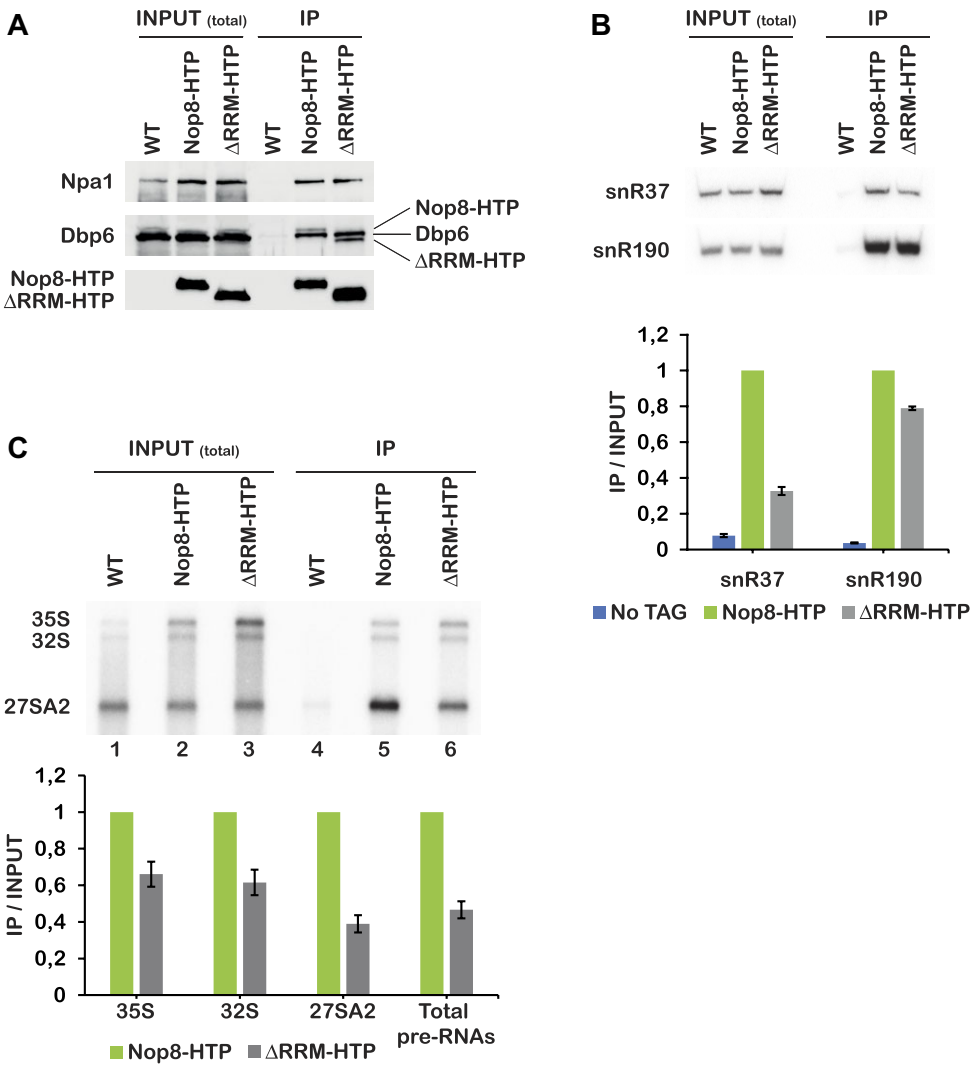


**Figure 3.** The RRM domain is dispensable for Nop8 interaction with snR190 snoRNA but strengthens Nop8 association with pre-rRNAs. Immunoprecipitation experiments were carried out using IgG Sepharose and extracts from the parental W303 WT strain (WT), a strain expressing Nop8-HTP [i.e. Nop8 bearing a C-terminal (His)6 tag, followed by a TEV cleavage site and two IgG-binding Z domains of *S. aureus* protein A] or Nop8ΔRRM-HTP (ΔRRM-HTP). Total proteins or RNAs were extracted from input extracts [INPUT (total)] or from immunoprecipitated samples (IP) and analysed by western blot (A) or northern blot (B, C). (**A**) Nop8-HTP and Nop8ΔRRM-HTP were detected using PAP, Npa1 and Dbp6 with specific antibodies. (**B**) The indicated snoRNAs were detected with specific antisense oligonucleotide probes. Quantification of northern data is presented in the histogram below the northern blot. Ratios of precipitated snoRNAs versus snoRNAs present in the input extracts (IP/INPUT) were computed from phosphorimager scans of northern membranes. Ratios obtained for the strain expressing Nop8-HTP were arbitrarily set at 1. Error bars correspond to standard deviations computed from two technical replicates. (**C**) The indicated pre-rRNAs were detected using the 23S1 probe. Quantification of northern data is presented in the histogram below the northern blot. Ratios of precipitated pre-rRNAs versus input pre-rRNAs (IP/INPUT) were computed from phosphorimager scans of northern membranes. Ratios obtained for the strain expressing Nop8-HTP were arbitrarily set at 1. Error bars correspond to standard deviations computed from two technical replicates.

cles (Fig. 4B). Interestingly, the weakened association of Nop8ΔRRM, and as a consequence of snR190 snoRNA, with pre-ribosomal particles was correlated with a pre-rRNA processing phenotype, characterized by a 30% drop of the 27SB pre-rRNA/27SA2 pre-rRNA ratio when compared with the WT control (Fig. 4C). A weakened association of Nop8ΔRRM with pre-ribosomal particles could result in reduced accumulation within the nucleolus. To test this, we expressed from a plasmid Nop8ΔRRM tagged with NeonGreen (Nop8ΔRRM-NG) in cells depleted of endogenous Nop8, or WT Nop8 bearing the same tag (Nop8-NG) as control (Fig. 4D). Indeed, Nop8ΔRRM was less concentrated in the nucleolus, labelled with Nop1-mCherry, than WT Nop8.

## The internal stem-loop structure of snR190 snoRNA plays a key role in its interaction with the isolated Npa1 complex

We next investigated which sequences of snR190 snoRNA are necessary for its specific interaction with the isolated Npa1 complex. According to our previous Npa1 CRAC dataset [10], Npa1 cross-linking sites are positioned within an internal stem-loop extension and within box B, which is complementary to 25S rRNA domain I (Fig. 5A). We therefore analysed the contribution of these regions of snR190 snoRNA to its interaction with the isolated Npa1 complex. We generated plasmids expressing snR190 mutants featuring nucleotide substitutions at the Npa1 cross-linking sites within

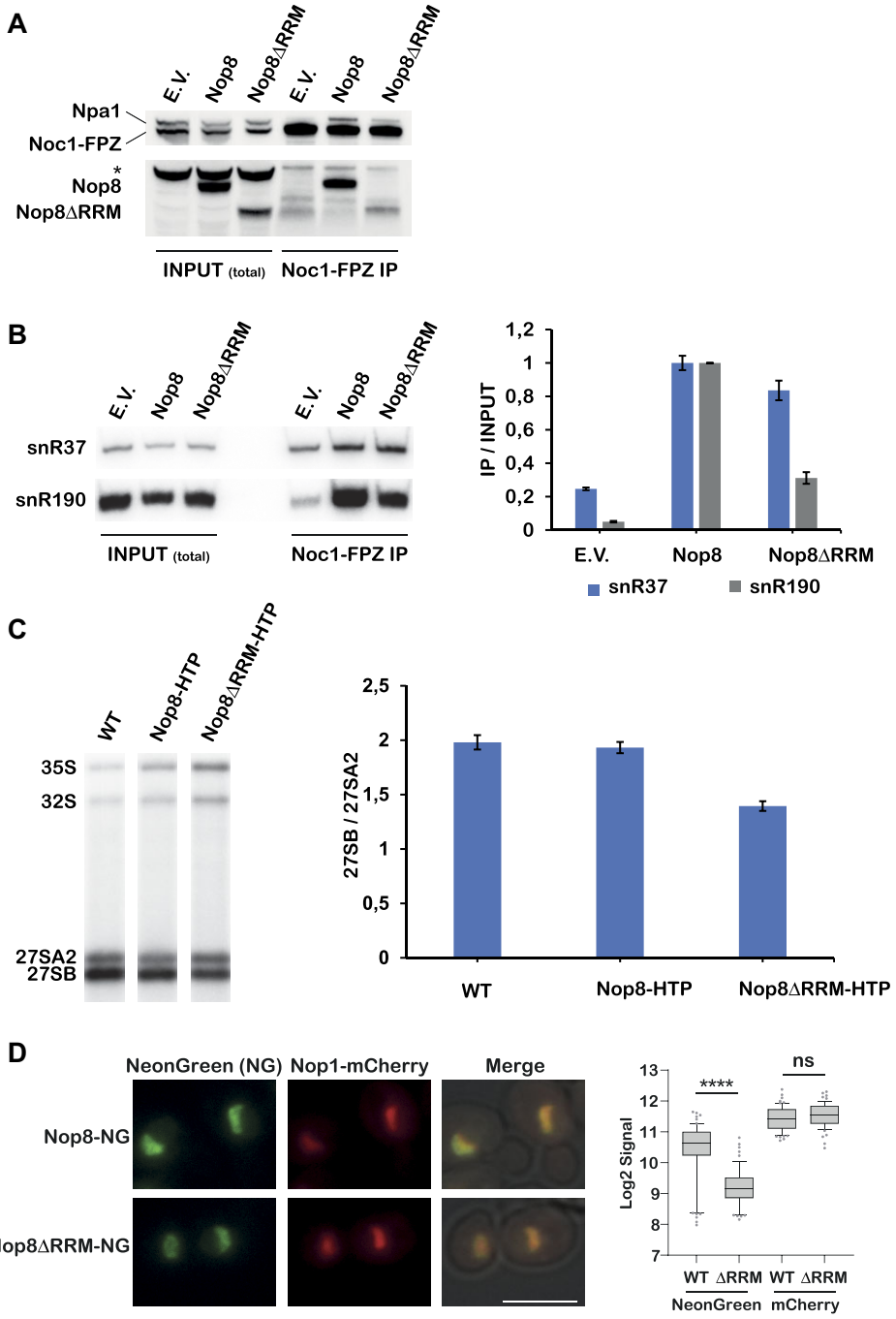


**Figure 4.** Effects of Nop8 RRM deletion on snR190 snoRNA association with pre-ribosomal particles and on pre-rRNA processing. (A, B) Immunoprecipitation experiments were carried out using IgG Sepharose and extracts from *GAL::HA-nop8/NOC1::FPZ* cells grown in glucose-containing medium for 14 h to deplete genome-encoded Nop8 and transformed with plasmids expressing WT Nop8 or Nop8ΔRRM, or an empty parental vector (E.V.). Total proteins or RNAs were extracted from input extracts [INPUT (total)] or from immunoprecipitated samples (Noc1-FPZ IP) and analysed by western blot (panel A) or northern blot (panel B). (**A**) Noc1-FPZ was detected using PAP, Npa1 and Nop8 with specific antibodies. The star highlights an unknown polypeptide detected by the anti-Nop8 serum. (**B**) snR37 and snR190 snoRNAs were detected with specific antisense oligonucleotide probes. Quantification of northern data is presented in the histogram on the right. Ratios of precipitated snoRNAs versus snoRNAs present in the input extracts (IP/INPUT) were computed from phosphorimager scans of northern membranes. Ratios obtained for the NOP8-expressing strain were arbitrarily set at 1. Error bars correspond to standard deviations computed from two technical replicates. (**C**) Total RNAs were extracted from the parental W303 WT strain, a strain expressing Nop8-HTP or Nop8ΔRRM-HTP and analysed by northern blot. The indicated pre-rRNAs were detected using the rRNA2.1 probe. Quantification of northern data is presented in the histogram on the right. Levels of 27SA2 and 27SB pre-rRNAs were obtained from phosphorimager scans of northern membranes. Shown are the ratios of 27SB/27SA2 pre-rRNA levels. Error bars correspond to standard deviations computed from three independent biological replicates. (**D**) Nop8 lacking the RRM domain exhibits decreased nucleolar localization. Strains expressing Nop1-mCherry and Nop8 or Nop8ΔRRM fused to NeonGreen (Nop8-NG or Nop8ΔRRM-NG, respectively) were grown exponentially and cells were analysed by fluorescence microscopy. Merge: overlay of signals. Scale bar: 5 μm. Right panel: box plot quantification ($Log_2$) of the NeonGreen signal present in the nucleolus or the mCherry signal of cells expressing Nop8-NG and Nop1-mCherry ($n = 56$) or Nop8ΔRRM and Nop1-mCherry ($n = 62$); *n*: number of cells pooled from three biologically independent replicates. Box limits: 25–75th percentiles; line: median; whiskers extend to 1.5 times the interquartile range on both ends. *P*-values were calculated with unpaired two-tailed Welch's *t*-test (****$P < .0001$; ns: not significant).

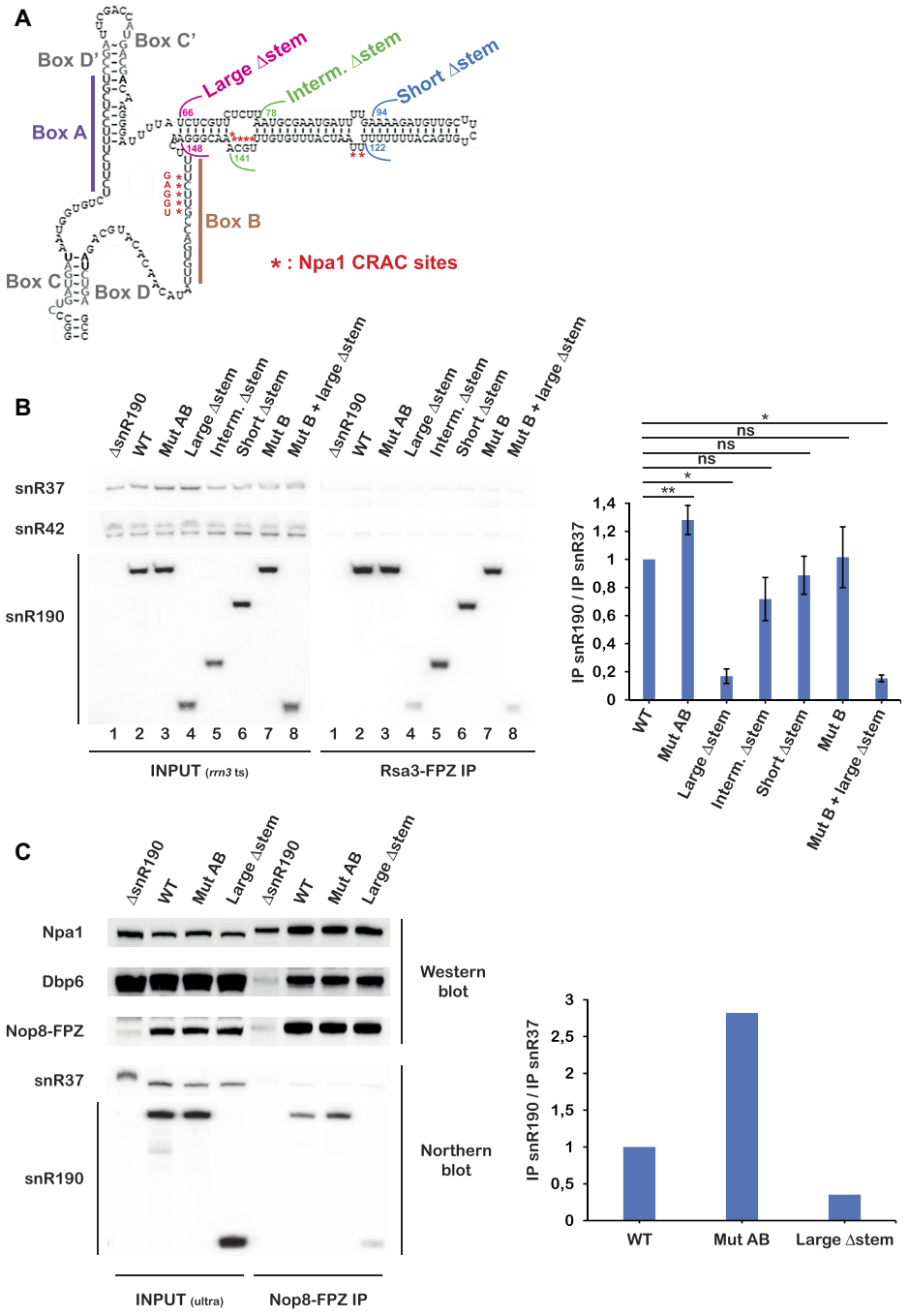


**Figure 5.** The internal stem-loop of snR190 is crucial for the interaction of snR190 snoRNA with the isolated Npa1 complex. (**A**) Secondary structure prediction of snR190 snoRNA with the positions of Npa1 cross-linking sites identified by CRAC. The sequence of the mutated box B of the snR190-[mut.B] mutant is indicated. The segments of the internal stem-loop removed in the various truncation mutants are indicated by brackets. (**B**) The *rrn3.8/RSA3::FPZ/snr190-[mut.C]* strains transformed with plasmids expressing WT snR190 snoRNA (WT), the indicated snR190 mutants or the empty vector (ΔsnR190) were grown for 4 h at 37°C to inactivate RNA Pol I transcription. Immunoprecipitation experiments were carried out with IgG Sepharose to precipitate Rsa3-FPZ. RNAs extracted from the total cellular extracts [INPUT (*rrn3* ts)] or immunoprecipitated samples (Rsa3-FPZ IP) were analysed by northern blot using probes detecting snR37, snR42, or snR190 snoRNAs. Quantification of the northern data is presented in the histogram on the right. Ratios of immunoprecipitated snR190 versus immunoprecipitated snR37 (IP snR190/IP snR37) were obtained from phosphorimager scans of northern membranes. The resulting ratios were normalized to the ratio obtained with WT snR190 snoRNA, arbitrarily set at 1. Error bars correspond to standard deviations, computed from three independent biological replicates. Statistically significant differences determined using one-tailed paired Student's *t*-test are indicated by asterisks (**$P < .01$; *$P < .1$; ns: not significant). (**C**) Extracts from the *NOP8::FPZ/snr190-[mut.C]* strains transformed with plasmids expressing WT snR190 snoRNA (WT), the indicated snR190 mutants or the empty vector (ΔsnR190) were subjected to two consecutive ultracentrifugation steps. Nop8-FPZ was precipitated from these extracts with IgG Sepharose. Total proteins or RNAs were extracted from input extracts [INPUT (ultra)] or from immunoprecipitated samples (Nop8-FPZ IP) and analysed by western blot (top panel) or northern blot (bottom panel), respectively. Nop8-FPZ was detected using PAP, Npa1 and Dbp6 with specific antibodies. The snR37 and snR190 snoRNAs were detected by northern blot using antisense oligonucleotide probes. Quantification of the northern data is presented in the histogram on the right. Ratios of immunoprecipitated snR190 versus immunoprecipitated snR37 (IP snR190/IP snR37) were obtained from phosphorimager scans of northern membranes. The resulting ratios were normalized to the ratio obtained with WT snR190, arbitrarily set at 1.

box B (snR190-[mut.B]), progressive truncations of the internal stem-loop (snR190-[short Δstem], snR190-[intermediate Δstem], and snR190-[large Δstem]), or featuring the box B mutations and lacking the internal stem-loop (snR190-[mut.B-large Δstem]). The snR190-[short Δstem] mutant retains all Npa1 cross-linking sites, while one cross-linking region is absent in snR190-[intermediate Δstem] and two in snR190-[large Δstem]. We also included in our analysis a mutant of snR190 snoRNA featuring mutations within boxes A and B (snR190-[mut.AB]) that abolish their complementarity to 25S rRNA domains I and V [16]. These snR190 mutations do not reduce snR190 steady-state levels (Supplementary Fig. S9). We then assessed the ability of snR190 snoRNA mutants to interact with the isolated Npa1 complex. To do so, plasmids expressing WT snR190 snoRNA or the above-described mutants were transformed into the *rrn3.8/RSA3::FPZ/snr190-[mut.C]* strain (which does not express snR190 snoRNA due to mutation of conserved box C, [16]). Rsa3-FPZ was precipitated from extracts of the transformed strains grown at 37°C to inactivate *de novo* ribosome biogenesis. Strikingly, the co-precipitation efficiency of snR190 snoRNA mutants lacking the internal stem-loop (snR190-[large Δstem] and snR190-[mut.B-large Δstem]) was reduced 10-fold relative to the WT situation (Fig. 5B, lanes 4 and 8). The co-precipitation efficiency of snR190-[intermediate Δstem] was also reduced, but to a far lesser extent. We conclude that the isolated Npa1 complex interacts with snR190 snoRNA to a large extent via its internal stem-loop structure.

As Nop8 can interact directly with the snR190 snoRNP in the absence of Npa1 complex formation, we asked whether the internal stem-loop of snR190 snoRNA is also important for the interaction with Nop8. We transformed a *NOP8::FPZ/snr190-[mut.C]* strain with the plasmids expressing WT snR190, snR190-[mut.AB], snR190-[large Δstem], or the empty parental vector. Nop8-FPZ was then precipitated from extracts subjected to two consecutive ultracentrifugation steps to pellet pre-ribosomal particles. Northern analysis indicated that the co-precipitation efficiency of snR190-[large Δstem] was reduced three-fold relative to WT snR190 snoRNA (Fig. 5C). Mutations of the A and B boxes led to an increase in snR190 snoRNA co-precipitation, which is likely due to reduced association with pre-ribosomal particles (Fig. 6). We conclude that the Nop8–snR190 snoRNA interaction involves major contacts with the internal stem-loop but other features of the snoRNP might also contribute to the interaction.

## The internal stem-loop of snR190 snoRNA is not essential for snR190 association with pre-ribosomal particles

We next investigated the contribution of snR190 snoRNA sequence elements to the stable integration of snR190 within pre-ribosomal particles. We transformed the plasmids expressing WT snR190 snoRNA and the above-described snR190 mutants into an *snr190-[mut.C]* strain expressing TAP-tagged Nop7, to allow precipitation of 90S and pre-60S particles. These particles were precipitated with Nop7-TAP with the same efficiency in all cases, as assessed by the western analysis of precipitated Nop7-TAP (Fig. 6A) and the northern analysis of precipitated pre-rRNAs (Supplementary Fig. S10). Mutations of both A and B boxes of snR190 snoRNA led to a 20% decrease in snR190 co-precipitation efficiency (Fig. 6B). In contrast, the large internal stem-loop deletion or the combination of the large stem-loop deletion and the box B mutations did not affect snR190 snoRNA co-precipitation efficiency (Fig. 6B). These results suggest that the ability of snR190 snoRNA to base pair with the pre-rRNA via either box A or B contributes to its stable integration within 90S/pre-60S pre-ribosomal particles but that its internal stem-loop structure has no influence. We also evaluated by western analysis the co-precipitation of Npa1, Dbp6, and Nop8 in cells expressing snR190-[mut.AB] or snR190-[large Δstem], as well as cells expressing WT snR190 snoRNA or lacking snR190 as controls (Fig. 6A). Lack of snR190 snoRNA internal stem-loop structure did not reduce the co-precipitation efficiency of Npa1, Dbp6, and Nop8. Altogether, these results suggest that the internal stem-loop structure of snR190 snoRNA is required neither for the integration nor for the retention of snR190 snoRNP and the Npa1 complex within pre-ribosomal particles.

## A strong interaction between the Npa1 complex and snR190 snoRNA is important for efficient pre-60S particle maturation

Removal of the internal stem-loop structure of snR190 snoRNA does not affect the association of snR190 snoRNA or Npa1 complex members with pre-ribosomal particles. Yet it strongly weakens the association between Npa1 complex members and snR190 snoRNA. This decreased association may impact pre-60S particle maturation. To test this hypothesis, we analysed by northern the effects of snR190 snoRNA mutations on pre-rRNA processing (Fig. 7). We observed, as previously reported [16], that the absence of snR190 snoRNA or the simultaneous mutation of both A and B boxes complementary to the pre-rRNA led to an increase in the levels of 27SA2 pre-rRNA and a decrease in 27SB pre-rRNA levels (Fig. 7, lanes 1, 2, and 3; see also Supplementary Fig. S1 for a scheme of pre-rRNA processing in *S. cerevisiae*). As a result, the 27SB/27SA2 ratio was halved when compared with the WT situation (Fig. 7). The deletion of snR190 snoRNA internal stem-loop also led to a similar, albeit less pronounced, pre-rRNA processing phenotype (Fig. 7, lanes 4 and 8), resulting in a 27SB/27SA2 ratio diminished by about 30% compared with the WT control. In contrast, the box B mutations or the short and intermediate deletions within the internal stem-loop had no significant impact on pre-rRNA processing (Fig. 7, lanes 5, 6, and 7). We also analysed the effects of these snR190 snoRNA mutations in cells lacking both snR190 and snR37, the two major snoRNA components of early pre-60S particles [5], to determine whether the lack of snR37 would exacerbate the effects of snR190 mutations. In fact, the pre-rRNA processing defects elicited by the snR190 snoRNA mutations were essentially identical in the *snr190-[mut.C]* and the *Δsnr37/snr190-[mut.C]* backgrounds (Supplementary Fig. S11). We note that the deletion of snR190 snoRNA internal stem-loop strongly weakens the direct interaction between the snR190 snoRNP and the Npa1 complex, while the box B mutations, or the short and intermediate internal stem deletions have no, or only a moderate effect on this interaction (Fig. 5). Our data therefore suggest that a direct, high-affinity interaction between snR190 snoRNP and the Npa1 complex within early pre-60S particles is required for their efficient maturation.

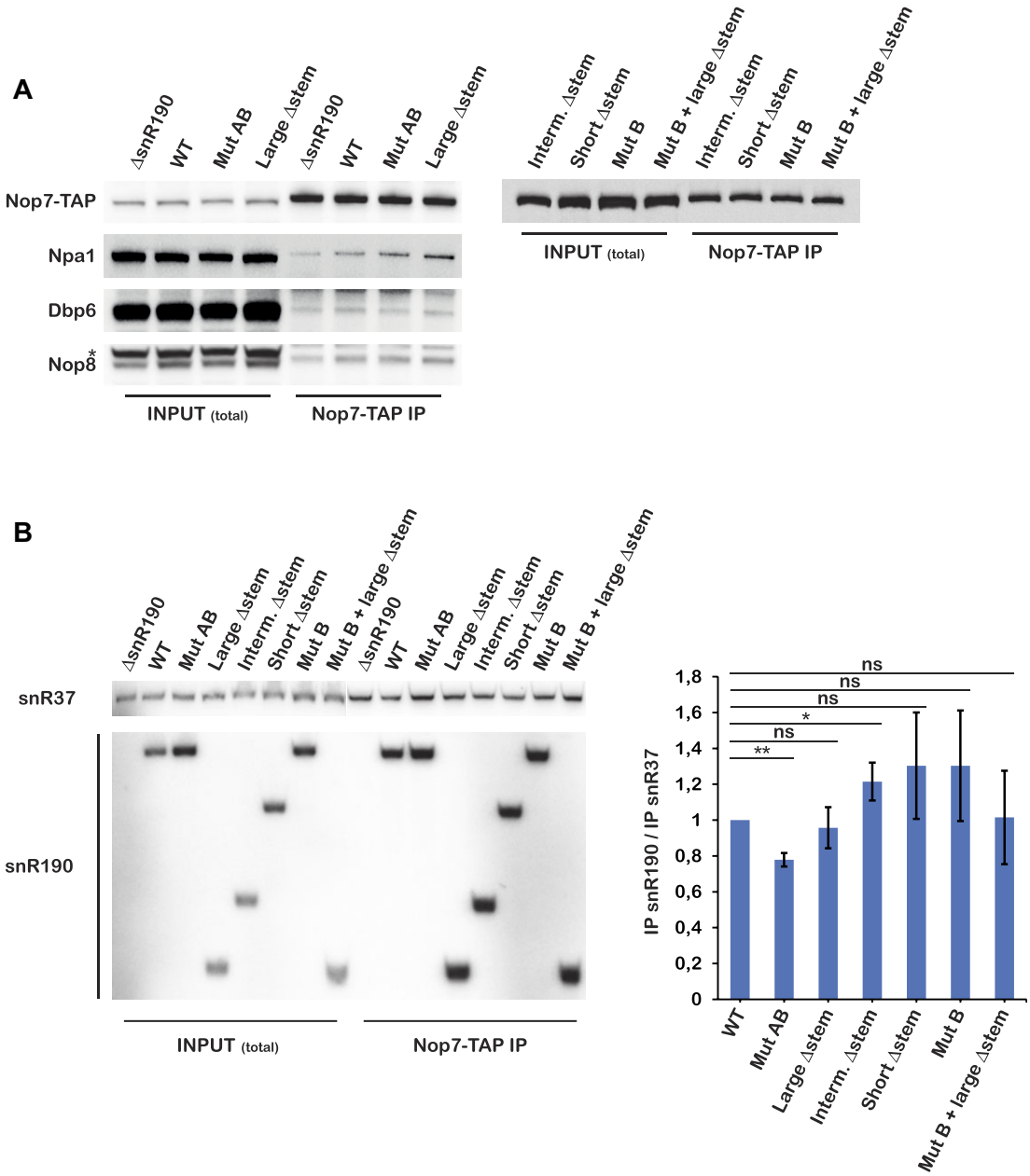


**Figure 6.** The internal stem-loop is not essential for snR190 snoRNA incorporation or retention within pre-60S particles. Immunoprecipitation experiments were carried out with IgG Sepharose and extracts from *NOP7::TAP/snr190-[mut.C]* strains transformed with plasmids expressing WT snR190 snoRNA (WT), the indicated snR190 mutants or the empty parental vector (ΔsnR190). Total proteins or RNAs were extracted from input extracts [INPUT (total)] or from immunoprecipitated samples (Nop7-TAP IP) and analysed by western blot (panel A) or northern blot (panel B), respectively. (**A**) Nop7-TAP was detected using PAP. For a subset of samples, Npa1, Dbp6, and Nop8 were also detected with specific antibodies. The star indicates an unknown polypeptide detected by the anti-Nop8 antibodies. (**B**) The snR37 and snR190 snoRNAs were detected by northern blot using antisense oligonucleotide probes. Quantification of the northern data is presented in the histogram on the right. Ratios of immunoprecipitated snR190 versus immunoprecipitated snR37 (IP snR190/IP snR37) were obtained from phosphorimager scans of northern membranes. The resulting ratios were normalized to the ratio obtained with WT snR190 snoRNA, arbitrarily set at 1. Error bars correspond to standard deviations, computed from three independent biological replicates. Statistically significant differences determined using one-tailed paired Student's *t*-test are indicated by asterisks (**$P < .01$; *$P < .1$; ns: not significant).

## Discussion

We report in this study the existence of an independent macromolecular assembly constituted by the Npa1 complex and the chaperone snoRNP snR190, two components of the first pre-60S particles that may help promote the folding and/or clustering of the 5′ and 3′ domains of 25S rRNA, and we investigated the nature of their interactions. We previously showed that lack of snR190 snoRNA weakens the association of Npa1 complex members with pre-ribosomal particles [16]. Here, we show that conversely, depletion of Npa1 or Nop8 severely weakens the association of snR190 snoRNA with pre-ribosomal particles. The effect seems more drastic and specific to snR190 in the case of Nop8 depletion. This finding may reflect a direct interaction between Nop8 and the snR190 snoRNP that may help recruit this snoRNP into

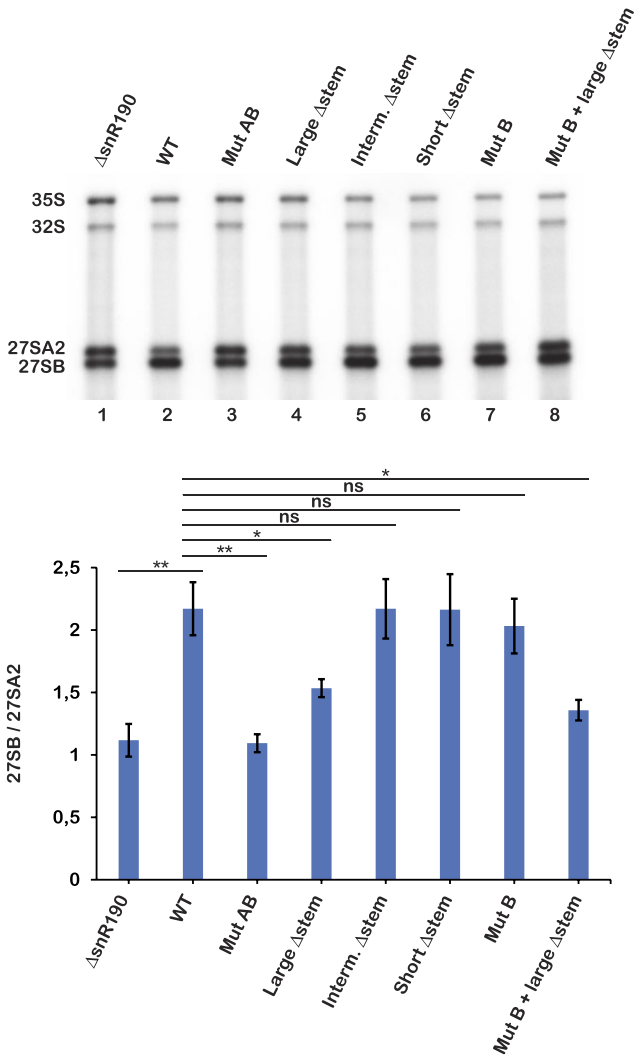


**Figure 7.** snR190 snoRNA internal stem-loop is important for normal pre-rRNA processing. Total RNAs were extracted from *snr190-[mut.C]* strains transformed with plasmids expressing WT snR190 snoRNA (WT), the indicated snR190 mutants, or the empty parental vector (ΔsnR190) and analysed by northern blot. The indicated pre-rRNAs were detected with the rRNA2.1 probe. Quantification of the northern data is presented in the histogram below the northern. Levels of 27SA2 and 27SB pre-rRNAs were obtained from phosphorimager scans of northern membranes. Shown are the ratios of 27SB/27SA2 pre-rRNA levels. Error bars correspond to standard deviations computed from three independent biological replicates. Statistically significant differences determined using one-tailed paired Student's *t*-test are indicated by asterisks (** $P < .01$; * $P < .1$; ns: not significant).

and/or tether it within pre-ribosomal particles. In contrast, Dbp6 depletion has little effect on snR190 snoRNA association with pre-ribosomal particles, although we cannot rule out the establishment of improper snR190/pre-rRNA interactions when the catalytic activity of the Npa1 complex is missing. CRAC data previously indicated that Npa1 directly binds snR190 snoRNA and that this snoRNA constitutes a major partner of Npa1 [10]. We now demonstrate that all members of the Npa1 complex interact with the snR190 snoRNA outside pre-ribosomal particles, that at least Nop1, a core protein of C/D box snoRNPs is present, therefore that a module constituted by the snR190 snoRNP bound to the Npa1 complex can be detected. Northern data and above all pCp labelling experiments strongly suggest that it is the only snoRNP that the Npa1 complex can interact with outside pre-ribosomal particles. To our knowledge, this is the first description of an independent macromolecular assembly involved in large-ribosomal-subunit synthesis constituted by a snoRNP chaperone bound to a defined protein complex. A similar macromolecular assembly involved in small subunit synthesis was already described for the snR30 snoRNP, which associates with AFs Kri1, Krr1, and Utp23 and RPs uS11 and uS15 [52, 53]. Utp23 and snR30 snoRNP together chaperone 18S rRNA folding and delivery of RPs uS11 and uS15 [53]. Another somewhat similar macromolecular assembly, containing the U3 snoRNP chaperone, nucleolin, Rrp5, and Dbp4, involved in small-ribosomal subunit synthesis in humans had also been previously described [54]. This assembly, whose full composition was not established, could only be detected when pre-rRNA transcription was blocked or when tUTP proteins were depleted.

Npa1 complex members are not required for normal accumulation of snR190 snoRNA, which is most probably stabilized by the canonical box C/D snoRNP proteins, consistent with the finding that box C mutations abolish snR190 snoRNA accumulation [16]. Moreover, it has been established that Nop58 and the methyltransferase Nop1, two core proteins of canonical box C/D snoRNPs, are components of the snR190 snoRNP [48, 55]. In accordance with these findings, we observed that Nop1 is co-purified with Rsa3 in the presence, but not in the absence of snR190 snoRNA. Conversely, lack of snR190 snoRNA does not weaken the association between Rsa3 and Npa1 complex members Npa1 and Dbp6. The absence of snR190 snoRNA does not prevent the association between Nop8 and Rsa3 either, but strikingly, while Nop8 depletion has no effect on snR190 snoRNA levels (see e.g. Fig. 1B), lack of snR190 snoRNA reduces Nop8 steady-state accumulation ([16], Figs 5C and 6A). This finding strengthens the hypothesis of a direct interaction between Nop8 and the snR190 snoRNP. One possible explanation is that binding of the snR190 snoRNP promotes/stabilizes Nop8 folding.

It remains unclear at present whether the snR190 snoRNP/Npa1 complex interaction is established prior to a common integration within pre-ribosomal particles or whether snR190 snoRNP and the Npa1 complex are released together from pre-ribosomal particles. Moreover, it is also possible that the snR190 snoRNP and the Npa1 complex may not associate prior to their integration into pre-ribosomal particles but are extracted together from these particles during the ultracentrifugation steps. However, the fact that the snR190 snoRNP/Npa1 complex module is also detected without ultracentrifugation of the extracts under conditions of RNA Pol I inhibition suggests that it exists in a free form in the cell. The interaction between the snR190 snoRNP and the Npa1 complex requires Npa1 and Nop8, but not Npa2. The requirement for Npa1 can be explained by the fact that this protein is essential for Npa1 complex formation and that it directly binds to snR190 snoRNA according to CRAC data [10]. Nop8 interacts directly with the free snR190 snoRNP in absence of Npa1 complex formation. It remains to be determined whether Nop8 solely binds to the snR190 snoRNA or whether it also interacts with snoRNP proteins. Interestingly in that respect, an interaction between Nop8 and Nop1, the methyltransferase component of box C/D snoRNPs, has been detected by a high-throughput cross-linking analysis [56]. We initially hypothesized that Nop8 RRM could help tether the

Npa1 complex to snR190 by a direct interaction with this snoRNA. However, our data demonstrate that the RRM is dispensable for Nop8 interaction with the free snR190 snoRNP. It contributes instead to the anchoring of Nop8 within pre-ribosomal particles, most probably via direct interaction(s) with the pre-rRNA.

The free snR190 snoRNP interacts with the Npa1 complex via, at least, Npa1 and Nop8. According to CRAC data, Npa1 establishes direct contacts with snR190 box B and with an internal stem-loop structure specific to snR190. Consistent with these binding sites, we found that removal of the entire stem-loop structure, and hence of two of the three Npa1 cross-linking regions, severely weakens the interaction outside pre-ribosomal particles between snR190 snoRNA and the Npa1 complex purified via Rsa3. When we used Nop8 as bait, we also detected a reduced interaction with snR190 snoRNA, which was, however, far less diminished than when the purification was performed with Rsa3. We suppose that Nop8 can still interact to a significant extent with the snR190 snoRNP lacking the internal stem-loop structure, maybe via Nop1 [56]. Nevertheless, our data clearly show that snR190 snoRNA internal stem-loop is a very important contributor to the interaction between the Npa1 complex and the snR190 snoRNP, at least outside pre-ribosomal particles. This stem-loop structure has been conserved in snR190 snoRNA homologues throughout Ascomycota, presumably due to its contribution to Npa1 complex binding [48]. The fact that removal of this structure does not affect the accumulation of snR190 snoRNA is consistent with the notion that Npa1 binding is not necessary for snR190 stability. We were somewhat surprised, however, that removal of the internal stem-loop structure of snR190 snoRNA has no effect on snR190 association with pre-ribosomal particles, as assessed by immunoprecipitation experiments with tagged Nop7 as bait. This undiminished co-precipitation with Nop7 of snR190 snoRNA lacking the internal stem-loop indicates that this structure is required neither for the integration, nor for the retention of snR190 snoRNA within pre-ribosomal particles. The association of truncated snR190 snoRNA with the pre-ribosomal particles may rely in part on the residual interaction with Nop8 and on base-pairing interactions with the pre-rRNA via box A. Indeed, the 20% reduction in co-precipitation efficiency with tagged Nop7 of snR190 snoRNA featuring mutations within boxes A and B suggests that snoRNA/pre-rRNA base-pairing interactions contribute to the stability of snR190 snoRNA association with pre-ribosomal particles. Our data also lead us to conclude that the removal of the internal stem-loop of snR190 snoRNA does not affect the integration or retention within pre-ribosomal particles of Npa1, Nop8, and Dbp6.

Hence, both snR190 snoRNA lacking the internal stem-loop structure and the Npa1 complex are present within pre-60S particles. Nevertheless, removal of this internal structure leads to a slightly aberrant pre-rRNA processing phenotype, characterized by reduced 27SB pre-rRNA levels relative to 27SA2 pre-rRNA levels. It is reminiscent of the defect induced by lack of snR190 snoRNA [16], although it is milder. This processing phenotype may indicate impaired maturation of 27SA2-containing pre-60S particles and/or reduced stability of 27SB-containing pre-60S particles. As the internal stem-loop structure of snR190 snoRNA is required for high-affinity binding between the Npa1 complex and the snR190 snoRNP outside pre-ribosomal particles, it is tempting to propose that its deletion will also reduce the strength of the interactions between the Npa1 complex and the snR190 snoRNP within pre-60S particles and cause the pre-rRNA processing defect described above. A direct and strong interaction between the Npa1 complex and the snR190 snoRNP, mediated by its internal stem-loop structure, within the 27SA2-containing pre-60S particles may be required for the snR190 snoRNP and/or the Npa1 complex to correctly exert their role in pre-rRNA folding. This snR190 snoRNP/Npa1 complex interaction may correctly position the entire module relative to the pre-rRNA and/or the proteins present in their vicinity within the particles. For example, in 25S rRNA domain I, the Npa1-binding site and the sequence complementary to snR190 snoRNA box B lie adjacent to the binding sites of Prp43, Rpl3, and Rrp5 [37, 38]. Available data suggest direct interactions between Prp43 and Npa1 and between Prp43 and Rrp5 [38, 57] and indicate that Rpl3 is placed in the vicinity of Npa1 complex members Npa1, Nop8, Dbp6, and Rsa3 [14]. In 25S rRNA domain V, Dbp6-, Npa1-, and Dbp7-binding sites and the sequence complementary to snR190 snoRNA box A lie adjacent to each other in or close to the peptidyl transferase centre [10, 15, 30]. Importantly, the structural proximities are also corroborated by genetic interactions. Synthetic enhanced or synthetic lethal interactions have been obtained when combining inactivation/mutation of genes encoding Npa1 complex members and genes encoding Rpl3, Dbp7, Dbp9, and Rbp95 [11, 14, 42]. Thus, incorrect interactions between the Npa1 complex and the snR190 snoRNP may have negative structural and functional impacts on the pre-60S particle neighbourhoods just described.

## Acknowledgements

We are grateful to B. Pertschy for the gift of the *Δsnr37* strain. We thank staff members of the LITC (Light Imaging Toulouse CBI) facility for support and all members of the Henry/Henras team for helpful discussions. We are grateful to Mia-Latifah Maronat, Morgane Pujol, and Christine Maheu for expert technical assistance. We thank Augustin Le Mière for experimental help.

*Author contributions*: H.H. and Y.H. performed the bulk of the experimental work and data analysis, with strong contributions from M.J., C.D., J.B., A.M.-G., D.K., and B.A. to plasmid and strain construction, A.K. to immunoprecipitation experiments, and A.K.H. to sucrose gradient sedimentation experiments. B.A. performed the fluorescence microscopy, and P.E.S., C.P.-C., and O.H. performed structure prediction analyses. The research was supervised by Y.H. and A.K.H. The manuscript was written by Y.H. and revised by A.K.H., with input from all co-authors, in particular from D.K. All authors have read and agreed to the published version of the manuscript.

## Supplementary data

Supplementary data is available at NAR online.

## Conflict of interest

None declared.

## Funding

Agence Nationale de la Recherche (ANR) [ANR-20-CE12-0026] (to Y.H. and A.K.H.); CNRS and Toulouse University (to Y.H., A.K.H., and C.P.-C.); [ANR-21-CE12-0008-01] (to B.A.); Institut National du Cancer (INCA) [PLBIO-2020-091], [ANR-22-CE12-0009], and Accreditation from La Ligue Nationale Contre le Cancer (to C.P.-C. and P.E.S.); Swiss National Science Foundation (SNSF) [project grant 310030_204801] (to D.K.).

H.H. is supported by a Ph.D. fellowship from Toulouse University and La Ligue Nationale Contre Le Cancer. M.J. was supported by a Ph.D. fellowship from the Lebanese University and CIOES Organization. A.K. was supported by a Ph.D. fellowship from Toulouse University. Funding to pay the Open Access publication charges for this article was provided by ANR [ANR-20-CE12-0026].

## Data availability

Data supporting the findings of this study are available from the corresponding authors upon reasonable request.

## References

1. Dragon F, Gallagher JE, Compagnone-Post PA *et al.* A large nucleolar U3 ribonucleoprotein required for 18S ribosomal RNA biogenesis. *Nature* 2002;**417**:967–70. https://doi.org/10.1038/nature00769
2. Grandi P, Rybin V, Bassler J *et al.* 90S pre-ribosomes include the 35S pre-rRNA, the U3 snoRNP, and 40S subunit processing factors but predominantly lack 60S synthesis factors. *Mol Cell* 2002;**10**:105–15. https://doi.org/10.1016/S1097-2765(02)00579-8
3. Osheim YN, French SL, Keck KM *et al.* Pre-18S ribosomal RNA is structurally compacted into the SSU processome prior to being cleaved from nascent transcripts in *Saccharomyces cerevisiae*. *Mol Cell* 2004;**16**:943–54. https://doi.org/10.1016/j.molcel.2004.11.031
4. Cheng J, Lau B, La Venuta G *et al.* 90S pre-ribosome transformation into the primordial 40S subunit. *Science* 2020;**369**:1470–6. https://doi.org/10.1126/science.abb4119
5. Ismail S, Flemming D, Thoms M *et al.* Emergence of the primordial pre-60S from the 90S pre-ribosome. *Cell Rep* 2022;**39**:110640. https://doi.org/10.1016/j.celrep.2022.110640
6. Bassler J, Hurt E. Eukaryotic ribosome assembly. *Annu Rev Biochem* 2019;**88**:281–306. https://doi.org/10.1146/annurev-biochem-013118-110817
7. Klinge S, Woolford JL Jr. Ribosome assembly coming into focus. *Nat Rev Mol Cell Biol* 2019;**20**:116–31. https://doi.org/10.1038/s41580-018-0078-y
8. Dez C, Froment C, Noaillac-Depeyre J *et al.* Npa1p, a component of very early pre-60S ribosomal particles, associates with a subset of small nucleolar RNPs required for peptidyl transferase center modification. *Mol Cell Biol* 2004;**24**:6324–37. https://doi.org/10.1128/MCB.24.14.6324-6337.2004
9. Hierlmeier T, Merl J, Sauert M *et al.* Rrp5p, Noc1p and Noc2p form a protein module which is part of early large ribosomal subunit precursors in *S. cerevisiae*. *Nucleic Acids Res* 2013;**41**:1191–210. https://doi.org/10.1093/nar/gks1056
10. Joret C, Capeyrou R, Belhabich-Baumas K *et al.* The Npa1p complex chaperones the assembly of the earliest eukaryotic large ribosomal subunit precursor. *PLoS Genet* 2018;**14**:e1007597. https://doi.org/10.1371/journal.pgen.1007597
11. Rosado IV, Dez C, Lebaron S *et al.* Characterization of *Saccharomyces cerevisiae* Npa2p (Urb2p) reveals a low-molecular-mass complex containing Dbp6p, Npa1p (Urb1p), Nop8p, and Rsa3p involved in early steps of 60S ribosomal subunit biogenesis. *Mol Cell Biol* 2007;**27**:1207–21. https://doi.org/10.1128/MCB.01523-06
12. Miles TD, Jakovljevic J, Horsey EW *et al.* Ytm1, Nop7, and Erb1 form a complex necessary for maturation of yeast 66S preribosomes. *Mol Cell Biol* 2005;**25**:10419–32. https://doi.org/10.1128/MCB.25.23.10419-10432.2005
13. Tang L, Sahasranaman A, Jakovljevic J *et al.* Interactions among Ytm1, Erb1, and Nop7 required for assembly of the Nop7-subcomplex in yeast preribosomes. *MBoC* 2008;**19**:2844–56. https://doi.org/10.1091/mbc.e07-12-1281
14. Bhutada P, Favre S, Jaafar M *et al.* Rbp95 binds to 25S rRNA helix H95 and cooperates with the Npa1 complex during early pre-60S particle maturation. *Nucleic Acids Res* 2022;**50**:10053–77. https://doi.org/10.1093/nar/gkac724
15. Khreiss A, Capeyrou R, Lebaron S *et al.* The DEAD-box protein Dbp6 is an ATPase and RNA annealase interacting with the peptidyl transferase center (PTC) of the ribosome. *Nucleic Acids Res* 2023; https://doi.org/10.1093/nar/gkac1196
16. Jaafar M, Contreras J, Dominique C *et al.* Association of snR190 snoRNA chaperone with early pre-60S particles is regulated by the RNA helicase Dbp7 in yeast. *Nat Commun* 2021;**12**:744–64. https://doi.org/10.1038/s41467-021-26207-w
17. Kater L, Thoms M, Barrio-Garcia C *et al.* Visualizing the assembly pathway of nucleolar pre-60S ribosomes. *Cell* 2017;**171**:1599–1610. https://doi.org/10.1016/j.cell.2017.11.039
18. Sanghai ZA, Miller L, Molloy KR *et al.* Modular assembly of the nucleolar pre-60S ribosomal subunit. *Nature* 2018;**556**:126–9. https://doi.org/10.1038/nature26156
19. Zhou D, Zhu X, Zheng S *et al.* Cryo-EM structure of an early precursor of large ribosomal subunit reveals a half-assembled intermediate. *Protein & Cell* 2019;**10**:120–30.
20. Burlacu E, Lackmann F, Aguilar LC *et al.* High-throughput RNA structure probing reveals critical folding events during early 60S ribosome assembly in yeast. *Nat Commun* 2017;**8**:714. https://doi.org/10.1038/s41467-017-00761-8
21. Sanghai ZA, Piwowarczyk R, Broeck AV *et al.* A co-transcriptional ribosome assembly checkpoint controls nascent large ribosomal subunit maturation. *Nat Struct Mol Biol* 2023;**30**:594–9. https://doi.org/10.1038/s41594-023-00947-3
22. Venema J, Tollervey D. RRP5 is required for formation of both 18S and 5.8S rRNA in yeast. *EMBO J* 1996;**15**:5701–14. https://doi.org/10.1002/j.1460-2075.1996.tb00954.x
23. Milkereit P, Gadal O, Podtelejnikov A *et al.* Maturation and intranuclear transport of pre-ribosomes requires Noc proteins. *Cell* 2001;**105**:499–509. https://doi.org/10.1016/S0092-8674(01)00358-0
24. Bruning L, Hackert P, Martin R *et al.* RNA helicases mediate structural transitions and compositional changes in pre-ribosomal complexes. *Nat Commun* 2018;**9**:5383. https://doi.org/10.1038/s41467-018-07783-w
25. Combs DJ, Nagel RJ, Ares M Jr *et al.* Prp43p is a DEAH-box spliceosome disassembly factor essential for ribosome biogenesis. *Mol Cell Biol* 2006;**26**:523–34. https://doi.org/10.1128/MCB.26.2.523-534.2006
26. Lebaron S, Froment C, Fromont-Racine M *et al.* The splicing ATPase prp43p is a component of multiple preribosomal particles. *Mol Cell Biol* 2005;**25**:9269–82. https://doi.org/10.1128/MCB.25.21.9269-9282.2005
27. Leeds NB, Small EC, Hiley SL *et al.* The splicing factor Prp43p, a DEAH box ATPase, functions in ribosome biogenesis. *Mol Cell Biol* 2006;**26**:513–22. https://doi.org/10.1128/MCB.26.2.513-522.2006
28. Weaver PL, Sun C, Chang TH. Dbp3p, a putative RNA helicase in *Saccharomyces cerevisiae*, is required for efficient pre-rRNA processing predominantly at site A3. *Mol Cell Biol* 1997;**17**:1354–65. https://doi.org/10.1128/MCB.17.3.1354
29. Daugeron MC, Linder P. Dbp7p, a putative ATP-dependent RNA helicase from *Saccharomyces cerevisiae*, is required for 60S

ribosomal subunit assembly. *RNA* 1998;**4**:566–81. https://doi.org/10.1017/S1355838298980190
30. Aquino GRR, Hackert P, Krogh N *et al.* The RNA helicase Dbp7 promotes domain V/VI compaction and stabilization of inter-domain interactions during early 60S assembly. *Nat Commun* 2021;**12**:6152. https://doi.org/10.1038/s41467-021-26208-9
31. Daugeron MC, Kressler D, Linder P. Dbp9p, a putative ATP-dependent RNA helicase involved in 60S-ribosomal-subunit biogenesis, functionally interacts with Dbp6p. *RNA* 2001;**7**:1317–34. https://doi.org/10.1017/S1355838201010640
32. Berges T, Petfalski E, Tollervey D *et al.* Synthetic lethality with fibrillarin identifies NOP77p, a nucleolar protein required for pre-rRNA processing and modification. *EMBO J* 1994;**13**:3136–48. https://doi.org/10.1002/j.1460-2075.1994.tb06612.x
33. Sun C, Woolford JL Jr. The yeast NOP4 gene product is an essential nucleolar protein required for pre-rRNA processing and accumulation of 60S ribosomal subunits. *EMBO J* 1994;**13**:3127–35. https://doi.org/10.1002/j.1460-2075.1994.tb06611.x
34. Kressler D, de la Cruz J, Rojo M *et al.* Dbp6p is an essential putative ATP-dependent RNA helicase required for 60S-ribosomal-subunit assembly in *Saccharomyces cerevisiae*. *Mol Cell Biol* 1998;**18**:1855–65. https://doi.org/10.1128/MCB.18.4.1855
35. Rosado IV, de la Cruz J. Npa1p is an essential trans-acting factor required for an early step in the assembly of 60S ribosomal subunits in *Saccharomyces cerevisiae*. *RNA* 2004;**10**:1073–83. https://doi.org/10.1261/rna.7340404
36. Granneman S, Kudla G, Petfalski E *et al.* Identification of protein binding sites on U3 snoRNA and pre-rRNA by UV cross-linking and high-throughput analysis of cDNAs. *Proc Natl Acad Sci USA* 2009;**106**:9613–8. https://doi.org/10.1073/pnas.0901997106
37. Bohnsack MT, Martin R, Granneman S *et al.* Prp43 bound at different sites on the pre-rRNA performs distinct functions in ribosome synthesis. *Mol Cell* 2009;**36**:583–92. https://doi.org/10.1016/j.molcel.2009.09.039
38. Lebaron S, Segerstolpe A, French SL *et al.* Rrp5 binding at multiple sites coordinates pre-rRNA processing and assembly. *Mol Cell* 2013;**52**:707–19. https://doi.org/10.1016/j.molcel.2013.10.017
39. Shan L, Xu G, Yao RW *et al.* Nucleolar URB1 ensures 3′ ETS rRNA removal to prevent exosome surveillance. *Nature* 2023;**615**:526–34. https://doi.org/10.1038/s41586-023-05767-5
40. Henras A, Dez C, Noaillac-Depeyre J *et al.* Accumulation of H/ACA snoRNPs depends on the integrity of the conserved central domain of the RNA-binding protein Nhp2p. *Nucleic Acids Res* 2001;**29**:2733–46. https://doi.org/10.1093/nar/29.13.2733
41. Pausch P, Singh U, Ahmed YL *et al.* Co-translational capturing of nascent ribosomal proteins by their dedicated chaperones. *Nat Commun* 2015;**6**:7494. https://doi.org/10.1038/ncomms8494
42. de la Cruz J, Lacombe T, Deloche O *et al.* The putative RNA helicase Dbp6p functionally interacts with Rpl3p, Nop8p and the novel trans-acting factor Rsa3p during biogenesis of 60S ribosomal subunits in *Saccharomyces cerevisiae*. *Genetics* 2004;**166**:1687–99. https://doi.org/10.1093/genetics/166.4.1687
43. Panchaud N, Peli-Gulli MP, De Virgilio C. Amino acid deprivation inhibits TORC1 through a GTPase-activating protein complex for the Rag family GTPase Gtr1. *Sci Signal* 2013;**6**:ra42. https://doi.org/10.1126/scisignal.2004112
44. Longtine MS, McKenzie A 3rd, Demarini DJ *et al.* Additional modules for versatile and economical PCR-based gene deletion and modification in *Saccharomyces cerevisiae*. *Yeast* 1998;**14**:953–61. https://doi.org/10.1002/(SICI)1097-0061(199807)14:10%3c953::AID-YEA293%3e3.0.CO;2-U
45. Berger AB, Cabal GG, Fabre E *et al.* High-resolution statistical mapping reveals gene territories in live yeast. *Nat Methods* 2008;**5**:1031–7. https://doi.org/10.1038/nmeth.1266
46. Guglielmi B, Werner M. The yeast homolog of human PinX1 is involved in rRNA and small nucleolar RNA maturation, not in telomere elongation inhibition. *J Biol Chem* 2002;**277**:35712–9. https://doi.org/10.1074/jbc.M205526200
47. Dominique C, Maiga NK, Mendez-Godoy A *et al.* The dual life of disordered lysine-rich domains of snoRNPs in rRNA modification and nucleolar compaction. *Nat Commun* 2024;**15**:9415. https://doi.org/10.1038/s41467-024-53805-1
48. van Nues RW, Granneman S, Kudla G *et al.* Box C/D snoRNP catalysed methylation is aided by additional pre-rRNA base-pairing. *EMBO J* 2011;**30**:2420–30. https://doi.org/10.1038/emboj.2011.148
49. Henras A, Henry Y, Bousquet-Antonelli C *et al.* Nhp2p and Nop10p are essential for the function of H/ACA snoRNPs. *EMBO J* 1998;**17**:7078–90. https://doi.org/10.1093/emboj/17.23.7078
50. Santos MC, Goldfeder MB, Zanchin NI *et al.* The essential nucleolar yeast protein Nop8p controls the exosome function during 60S ribosomal subunit maturation. *PLoS One* 2011;**6**:e21686. https://doi.org/10.1371/journal.pone.0021686
51. Daubner GM, Clery A, Allain FH. RRM–RNA recognition: NMR or crystallography…and new findings. *Curr Opin Struct Biol* 2013;**23**:100–8. https://doi.org/10.1016/j.sbi.2012.11.006
52. Hoareau-Aveilla C, Fayet-Lebaron E, Jady BE *et al.* Utp23p is required for dissociation of snR30 small nucleolar RNP from preribosomal particles. *Nucleic Acids Res* 2012;**40**:3641–52. https://doi.org/10.1093/nar/gkr1213
53. Fischer P, LB T.M., Denk T *et al.* H/ACA snoRNP guides ribosomal RNA subdomain folding in a satellite particle before joining the core 90S pre-ribosome. bioRxiv, https://doi.org/10.1101/2024.09.05.611419, 7 September 2024, preprint: not peer reviewed.
54. Turner AJ, Knox AA, Prieto JL *et al.* A novel small-subunit processome assembly intermediate that contains the U3 snoRNP, nucleolin, RRP5, and DBP4. *Mol Cell Biol* 2009;**29**:3007–17. https://doi.org/10.1128/MCB.00029-09
55. Balakin AG, Smith L, Fournier MJ. The RNA world of the nucleolus: two major families of small RNAs defined by different box elements with related functions. *Cell* 1996;**86**:823–34. https://doi.org/10.1016/S0092-8674(00)80156-7
56. Sailer C, Jansen J, Sekulski K *et al.* A comprehensive landscape of 60S ribosome biogenesis factors. *Cell Rep* 2022;**38**:110353. https://doi.org/10.1016/j.celrep.2022.110353
57. Bassler J, Ahmed YL, Kallas M *et al.* Interaction network of the ribosome assembly machinery from a eukaryotic thermophile. *Protein Sci* 2017;**26**:327–42. https://doi.org/10.1002/pro.3085

**Received:** August 30, 2024. **Revised:** February 1, 2025. **Editorial Decision:** February 3, 2025. **Accepted:** February 12, 2025